The British Journal of Radiology, 84 (2011), S127–S144

Imaging biomarkers of angiogenesis and the microvascular environment in cerebral tumours

G THOMPSON, MBChB, MRCS, S J MILLS, PhD, FRCR, D J COOPE, PhD, MRCS, J P B O'CONNOR, PhD, FRCR and A JACKSON, FRCR, FRCP

Wolfson Molecular Imaging Centre, University of Manchester, Withington, Manchester, UK

ABSTRACT. Conventional contrast-enhanced CT and MRI are now in routine clinical use for the diagnosis, treatment and monitoring of diseases in the brain. The presence of contrast enhancement is a proxy for the pathological changes that occur in the normally highly regulated brain vasculature and blood-brain barrier. With recognition of the limitations of these techniques, and a greater appreciation for the nuanced mechanisms of microvascular change in a variety of pathological processes, novel techniques are under investigation for their utility in further interrogating the microvasculature of the brain. This is particularly important in tumours, where the reliance on angiogenesis (new vessel formation) is crucial for tumour growth, and the resulting microvascular configuration and derangement has profound implications for diagnosis, treatment and monitoring. In addition, novel therapeutic approaches that seek to directly modify the microvasculature require more sensitive and specific biological markers of baseline tumour behaviour and response. The currently used imaging biomarkers of angiogenesis and brain tumour microvascular environment are reviewed.

DOI: 10.1259/bjr/66316279

The advent of CT and MRI has enabled non-invasive evaluation of brain tumours, providing insights into their diagnosis, progression and therapeutic response. Advances in imaging techniques are shedding further light on tumour behaviour through imaging biomarkers of specific aspects of tumour vascular structure and function. In this review we will consider the current status of imaging techniques that are designed to study and quantify specific aspects of the angiogenic process and the properties of the resulting vasculature.

Microvasculature in cerebral tumours

Gliomas account for the majority of primary brain tumours, with glioblastoma multiforme (GBM) being the commonest subtype and conveying the poorest prognosis. The addition of adjuvant temozolomide chemotherapy to radiotherapy has improved median survival by only 2.5 months (from 12.1 to 14.6 months) over conventional radiotherapy and surgery [1]. Recurrence is inevitable with fewer than 1 in 6 surviving patients remaining progression free beyond 6 months and only 26.5% alive at 2 years [1]. Malignant gliomas exhibit a high degree of vascular proliferation histologically [2–4], and angiogenesis is a crucial, defining process in the progression of the disease [5]. As such, angiogenesis is one of the major therapeutic targets for the development of novel therapies. Microvascular proliferation and tumour heterogeneity increase with tumour grade. In addition to microvascular proliferation, GBMs exhibit areas of both high cellularity (due to dense cell packing and pseudopallisading) and low cellularity (secondary to necrosis). This is in contrast to grade II tumours with more diffuse spread of tumour cells and blood vessel architecture and density similar to that of normal brain, whereas grade III (anaplastic) tumours lie in between grade II and IV tumours, with more numerous tumour cells and occasional mitotic figures (Figure 1) [6].

Address correspondence to: Dr Alan Jackson, Wolfson Molecular Imaging Centre, 27 Palatine Rd, Withington, Manchester M20 3LJ, UK. E-mail: Alan.Jackson@manchester.ac.uk

Angiogenesis in gliomas

The vascular microenvironment of gliomas plays a major role in determining the pathophysiological characteristics of the tumour [7]. In order for a tumour to progress there must be an adequate blood supply to fuel growth, and as the tumour increases in size, so too must the blood supply to meet the increased nutrient demand. This process of neovascularisation is called angiogenesis, and is a major feature of high-grade tumours.

A vast number of growth factors have been implicated in glioma angiogenesis with vascular endothelial growth factor (VEGF) being attributed as the principal pro-angiogenic factor [8–10]. VEGF has endothelial mitogenic effects and promotes new capillary growth from existing vessels [11]. In addition to promoting neovascularisation it can also enhance microvascular permeability without causing endothelial cell damage [12] and can cause vasodilatation in normal vessels [13–15]. It was originally described as vascular permeability factor because of its ability to cause vascular leakage [16].

VEGF expression in glioma cells can be approximately 50 times that occurring in normal brain [17] and is directly related to glioma grade [18]. A number of events promote VEGF production. As new vessels grow there is

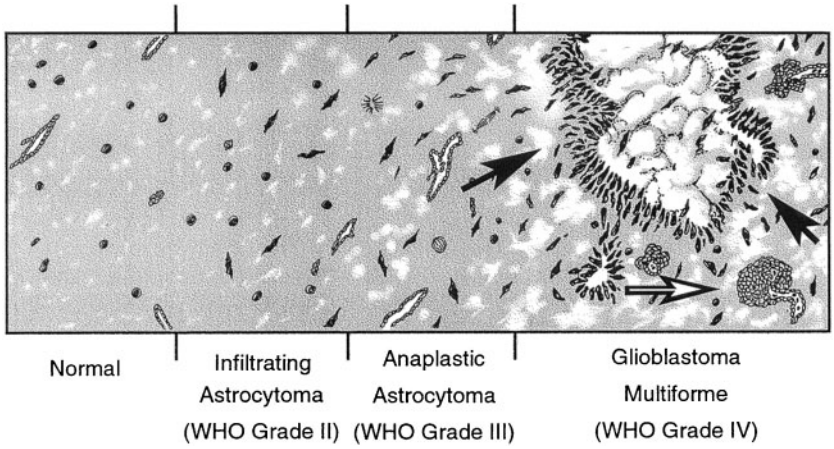

Figure 1. Schematic diagram showing the progression of a low-grade tumour to a high-grade glioblastoma multiforme. Black arrows indicate palisades of densely packed tumour cells adjacent to an area of necrosis. White arrow identifies an area of glomeruloid, abnormal microvascular proliferation.

endothelial hyperplasia, which in turn expresses more VEGF and promotes the growth of more vessels [6]. As tumour growth continues, fuelled with nutrients and oxygen from the neovasculature, it begins to outstrip its blood supply and oxygen levels fall. The ensuing cellular hypoxia causes a cascade of events including the production of the transcription factor, hypoxia inducible factor 1 alpha (HIF-1α) [19]. This, in turn, upregulates VEGF, promoting angiogenesis and perpetuating the vicious cycle of hypoxia, tumour growth and angiogenesis (Figure 2) [20]. The clinical importance of VEGF overexpression and its sequelae are related to the poor prognosis associated with a generally higher underlying grade of tumour [21–24].

The resulting neovasculature in gliomas is structurally and functionally abnormal [7], and irregularities of the endothelial lining result in increased blood–brain barrier (BBB) permeability [25, 26]. The morphology of the vessels varies within and between tumours, with vessel diameters ranging from 3 to 40 μm [7] and formation of microaneurysms and arteriovenous shunts. The topological architecture also becomes chaotic, with disorganised and tortuous vessels. Increased endothelial proliferation with higher numbers of fenestrations, a thickened basement membrane, and abnormal pericyte relationships culminate in a dysfunctional blood–tumour barrier (BTB) in stark contrast to the highly controlled BBB in parent capillaries. In addition, although morphologically similar in culture, isolated endothelial cells from high-grade glioma (HGG) exhibit substantially higher rates of proliferation than those from low-grade glioma (LGG).

The ability of tumour microcirculation to meet metabolic demands is based on both structural and physiological factors. Aberrant calibre, number and tortuosity reflect the culmination of abnormal angiogenesis during the growth of the tumour. This can be defined invasively through histological assessment—such as microvascular density (MVD), a standardised histopathological measure of the mean microvessel count under set microscopic conditions—although sampling error is common in light of heterogeneity, and longitudinal follow-up is implicitly precluded [27, 28]. The quality of perfusion also has a large impact on the tumour microenvironment and in gliomas, despite their highly angiogenic and vascularised nature, perfusion is more heterogeneous than that of normal grey and white matter [29, 30]. It has been shown in a mouse model of glioma, for example, that the vessels formed by neoangiogenesis are only 50–70% perfused in the periphery of the tumour, compared with >95% perfusion in the established capillary bed of normal brain

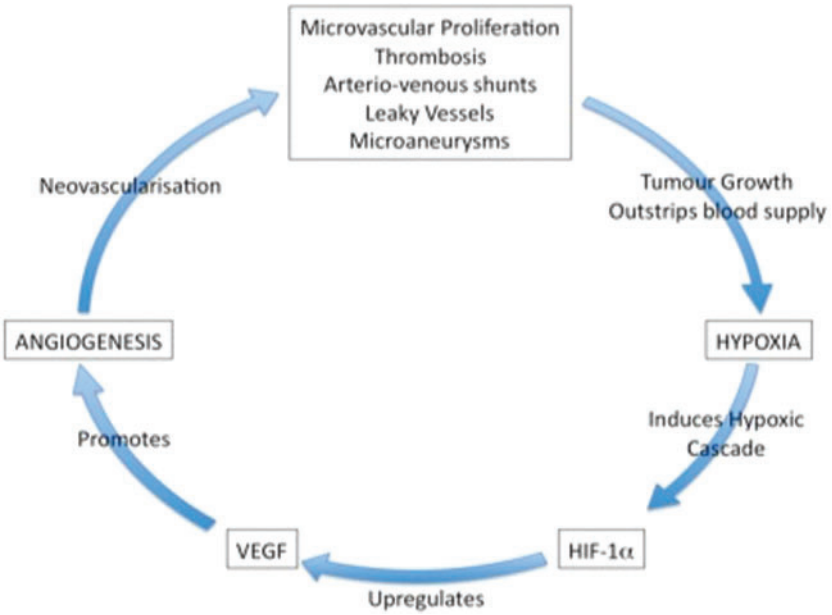

Figure 2. As tumour growth continues, fuelled with nutrients and oxygen from the neovasculature, it begins to outstrip its blood supply and oxygen levels fall. The ensuing cellular hypoxia causes a cascade of events including the production of the transcription factor, hypoxia inducible factor 1 alpha (HIF-1α) [19]. This, in turn, upregulates vascular endothelial growth factor (VEGF), promoting angiogenesis and perpetuating the vicious cycle of hypoxia, tumour growth and angiogenesis (reproduced from [6] with permission).

tissue. Moreover, within the partially necrotic centre of larger tumours fractional perfusion can be as low as 25% [31]. Other features of glioma vasculature dysfunction include hyperpermeability and disordered autoregulation [32–34]. Permeability is a result of both a fundamental difference in underlying vascular function, and the constantly changing influence of local and circulating factors on the BTB. It is advantageous, therefore, to be able to describe elements of permeability, blood volume and flow as distinct biomarkers. Each of these gives separate insights into the ongoing angiogenic process and any changes that result from or may influence treatment. Since histological methods are largely morphological, providing little information about perfusion, blood flow or vessel function, non-invasive imaging assessment of microvasculature is increasingly sought after, and this underlies the development and application of the techniques described in this review and elsewhere in this special issue.

Potential imaging biomarkers of angiogenesis

All major imaging modalities have been utilised in the investigation of tumour microvasculature, including CT, MR, single photon emission computed tomography (SPECT), positron emission tomography (PET), ultrasound and optical imaging. The last two are largely experimental, being used primarily in the intra-operative setting or in animal models of disease, and will not be discussed further. Other imaging techniques provide either direct biomarkers of microvascular structure and function or indirect markers that measure biochemical- or physiological-related processes. Indirect evidence of vascular status can be provided by metabolic imaging techniques that estimate metabolite profiles in the tumour and surrounding tissues; examples include amino acid (tyrosine and methionine) and nucleotide (thymidine) PET, which are correlated with vascular endothelial proliferation and nucleic acid turnover respectively [35]. Measures of hypoxia and glycolysis such as ^{18}FMISO (^{18}F-fluoromisonidazole) PET [36] and ^{1}H-MRS (proton magnetic resonance spectroscopy) also provide useful supportive data in many applications [37]. Early clinical work utilising hyperpolarised carbon-13 MR to produce maps of tissue pH may be useful in the management and follow-up of tumours but is severely limited by logistic availability.

The basic science principles and methodology behind these various techniques have been recently reviewed by Herholz et al [38] and are discussed in detail later in this special edition (Specific biomarkers of receptors, pathways of inhibition and targeted therapies, Parts I and II by Waerzeggers et al).

As described earlier, endothelial cells in HGG are more proliferative than those in LGG. [^{11}C]-methionine-uptake on PET has been correlated with MVD on microscopy and proposed as an indirect marker of angiogenesis [39]. Having previously demonstrated that methionine uptake correlates closely with relative cerebral blood volume (rCBV) in glioma, Sadeghi et al reported a correlation between increasing rCBV on dynamic susceptibility weighted MRI (DSC-MRI), endothelial proliferation and mitotic activity in stereotactic biopsies guided to regions of high methionine uptake [40, 41]. They also described a relationship between rising rCBV and an increase in both cellularity and MVD in bulk tumour biopsies, which was not apparent on diffusion-weighted imaging measures, which are often used as a proxy for cellular density [42].

Correlation has also been reported between DSC-MRI rCBV and glucose metabolism as measured by ^{18}FDG-PET [43], with correlation of maximum rCBV and maximum glucose uptake seen in all 21 gliomas, but voxel-by-voxel correlation seen in only 16 tumours. Unlike blood volume, blood flow and glucose uptake were relatively well matched. These functional parameters also correlated with morphological and immunohistological vascularity on biopsy. Using a combination of ^{18}F-FET (fluoro-ethyl-l-tyrosine) and $H_2{}^{15}O$ PET to determine the distribution of brain capillaries and cerebral blood flow (CBF) respectively in 17 LGGs, Wyss et al [44] demonstrated a highly heterogeneous distribution with spatial coincidence of flow and amino acid uptake at the centre of the tumours. Increased uptake at the infiltrating tumour edge was not coupled to increased flow, and such mismatches between tracer delivery and uptake have been suggested as markers for following response to treatment. Although indirect imaging measures can be technically demanding and can lack spatial resolution, there has been renewed interest in adjuncts to more direct microvascular imaging techniques owing to the confounding effects described with novel vascular-targeting therapeutics [159].

In general, the imaging modalities aimed at deriving direct information about vasculature and angiogenesis fit into two categories: molecular imaging and dynamic contrast-enhanced imaging.

Molecular imaging

Molecular imaging in gliomas is discussed in detail in other articles within this special edition. However, it is worthwhile briefly reviewing the available molecular imaging approaches that specifically target the angiogenic process. There is extensive interest in the development of PET and SPECT ligands that target specific aspects of the angiogenic process. A large number of candidate agents have been described and employed, almost exclusively in animal models. The major biological targets for angiogenesis-specific imaging agents are briefly discussed here.

Integrins

Integrins are a family of cell surface receptors that mediate the interactions between adjacent cells, or the cells and the intracellular matrix. They are known to play a key role in angiogenesis, including the proliferation, adhesion, differentiation and survival of endothelial cells [45]. Of the various integrins, most attention has been focused on $\alpha_v\beta_3$, which is upregulated in proliferating endothelial cells and poorly represented in quiescent vasculature. Since $\alpha_v\beta_3$ integrin binds proteins displaying the triple amino acid sequence arginine–glycine–aspartic acid (RGD) it is a candidate for targeted imaging. A recently published study [158] using a ^{18}F-labelled RGD peptide ([^{18}F]Galacto-RGD) in patients with glioblastoma showed negligible tracer accumulation in normal brain, whereas tumours demonstrated significant but heterogeneous tracer uptake. Immunohistochemical examination of tumour tissue showed close

correlation between ligand uptake and immunohistochemical expression of $\alpha_v\beta_3$, which were seen both on endothelial and primary tumour cells. This and other similar imaging agents, targeting one or more endothelial cell-expressed integrins, offer considerable promise in future studies where selective integrin-argeting agents are used for therapeutic benefit.

VEGF and other targets

A large number of studies have described potential imaging agents for the angiogenic process capable of detection using SPECT or more commonly PET imaging. To the best of our knowledge, none of these specific angiogenesis-targeting agents has so far been employed in glioma patients. Imaging of VEGF and, more commonly, VEGF receptors (VEGFRs) has been the subject of extensive study, and a number of pre-clinical imaging studies have been described. Similarly, endothelial cell surface receptors, which are regulated in malignancy, have been studied as potential imaging targets. Endostatin and angiostatin are naturally occurring proteins that act as potent angiogenesis inhibitors targeting endothelial cell proliferation [46]. Labelled versions of both of these proteins have been used in animal models to assess response to angiogenesis-targeted therapy. Matrix metalloproteinases (MMPs) are zinc-dependent enzymes that catalyse the breakdown of the extracellular matrix (ECM) components. They modify the ECM and, among other functions, unmask integrin binding sites. MMP overexpression is instrumental in tumour growth and invasion. Several MMP inhibitors (MMPIs) have been developed for anti-cancer therapy and the development of imaging ligands based on MMPIs is a topic of current research interest.

Dynamic contrast-enhanced imaging techniques

The majority of published studies using imaging biomarkers to probe the structure and function of tumour microvasculature have used dynamic contrast-enhanced methods. These techniques, described in detail elsewhere in this special issue, are similar. They use injection of an intravascular contrast agent combined with dynamic image acquisition to produce time course data, which show the behaviour of the contrast agent as it passes into a tissue of interest (Figure 3). The majority of published work has used dynamic contrast-enhanced MRI (DCE-MRI), although increasingly dynamic contrast-enhanced CT (DCE-CT) is being applied in clinical settings. DCE-MRI data may be acquired using either T_1 (dynamic relaxivity contrast-enhanced MRI, DRCE-MRI) or T_2* (dynamic susceptibility contrast-enhanced MRI; DSCE-MRI) weighted sequences. It is worth noting that there is some diversity in the nomenclature for dynamic MRI. While DRCE- and DSCE-MRI are the technically correct variants of DCE-MRI, the more generic DCE-MRI has been routinely adopted to refer to T_1 weighted or relaxivity-based techniques, and DSC-MRI is used to refer to susceptibility-based techniques, most commonly T_2* weighted. Specific biomarkers can be derived from these time course data using a variety of approaches. Semi-quantitative analyses looking at the degree or rate of change in signal intensity have been widely applied but lack physiological specificity. Quantitative analyses, using pharmacokinetic models of contrast distribution between the different tissue compartments, are widely employed. These pharmacokinetic analysis techniques give rise to a range of quantitative biomarkers with varying degrees of biological specificity (Figure 4). The most commonly employed in studies performed to date are listed and briefly described below.

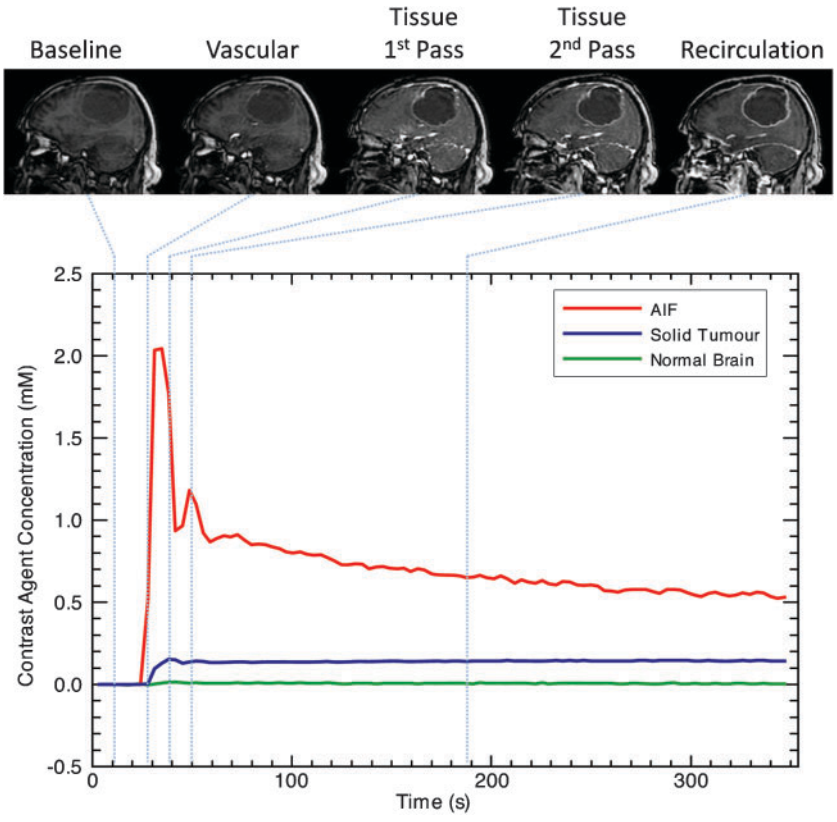

Figure 3. Time series of dynamic contrast-enhanced images and the contrast concentration curve. The dynamic series of images show the passage of the contrast agent bolus over a given time course. The changes in signal intensity are converted to changes in contrast agent concentration. The graph depicts changes in contrast agent concentration for three given regions of interest: carotid artery (red), to provide the arterial input function (AIF) for kinetic analysis solid enhancing tumour (blue) and normal appearing white matter (green).

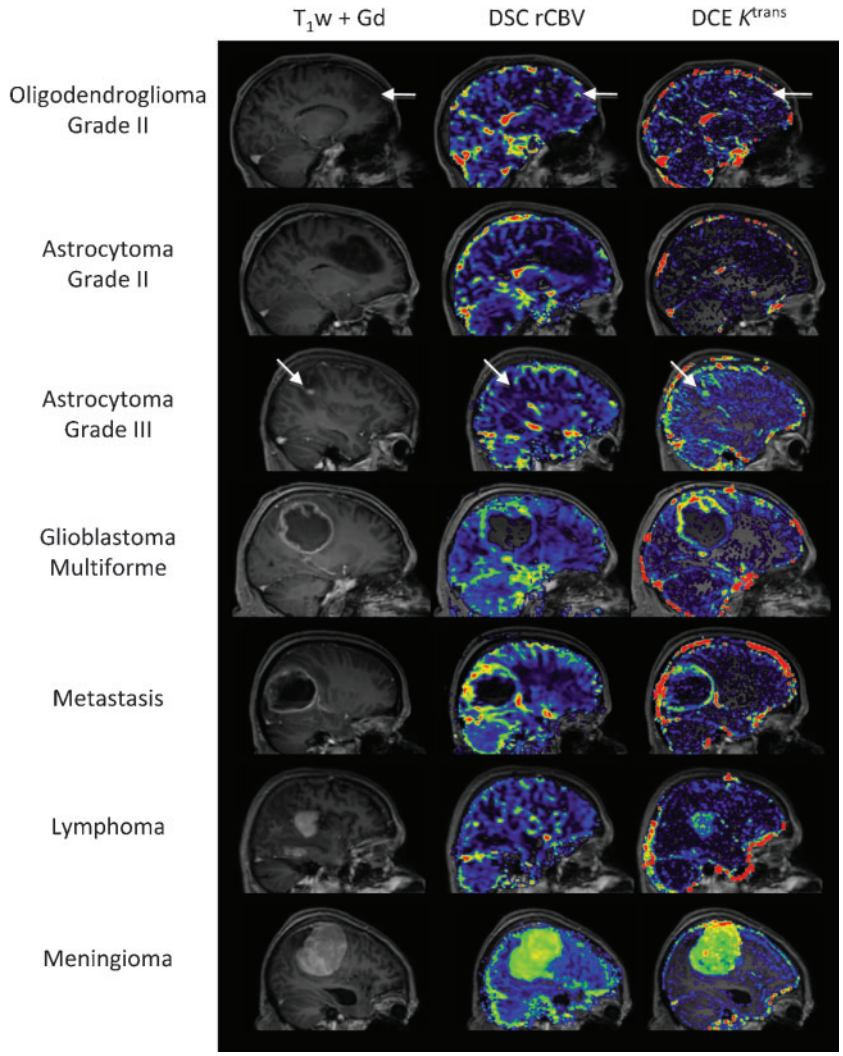

Figure 4. Examples of perfusion and permeability maps for a variety of histologically distinct intracranial tumours. Post-contrast T_1 weighted images and post-contrast T_1 weighted images with overlaid rCBV (cerebral blood volume) and K^{trans} maps for oligodendroglioma (O, grade II); there are focal increases in both rCBV and K^{trans} within the tumour (white arrows) when compared with normal appearing white matter; astrocytoma (A, grade II), both rCBV and K^{trans} within the tumour are similar to normal appearing white matter; anaplastic astrocytoma (AA, grade III), marked increase in K^{trans} and small increase in rCBV (white arrows) is seen within the tumour when compared with normal appearing white matter; glioblastoma multiforme (GBM, grade IV), the tumour exhibits both high rCBV and high K^{trans} within the solid enhancing component, with low/zero rCBV and K^{trans} within the necrotic core; metastasis (primary breast carcinoma), both rCBV and K^{trans} are elevated in comparison to normal appearing white matter; lymphoma, K^{trans} is elevated within the tumour mass while the rCBV remains similar to normal appearing white matter; and meningioma (grade I), the extremely high values of both rCBV and K^{trans} within the tumour in comparison to normal appearing white matter reflect the dural blood supply of the lesion, lying outside the blood–brain barrier. DCE, dynamic contrast enhanced; DSC, dynamic susceptibility weighted.

Cerebral blood volume

Cerebral blood volume (CBV) describes the proportion of each individual voxel that is represented by blood vessels. Most analysis techniques produce a unitless relative estimate of CBV that allows direct comparison between regions in the same subject. Between-subject comparison relies on normalisation of these values to a representative area of apparently ''normal'' tissue such as contralateral white matter or, more commonly, a large vein. Terminology can be confusing: the term *relative* cerebral blood volume is commonly used to describe values prior to normalisation. Unfortunately, normalised values are often referred to as *regional* blood volume and both are commonly abbreviated to rCBV. Current evidence suggests measurements of CBV from DSC-MRI and the equivalent metric from DCE-MRI (vascular fraction; v_p) are relatively similar [47, 48], although the behaviour of individual measurements is highly dependent on the imaging parameters for acquisition, and analytical approach applied to the data. In light of the logistical problems associated with dynamic MRI, recent work has addressed the use of other tissue contrast mechanisms for examining tumour vascularity. In particular, vascular space occupancy (VASO) imaging is a T_1 weighted technique using changes in measured T_1 to calculate blood volume changes in response to physiological stimuli [49, 50].

Contrast transfer coefficient

Most DCE-MRI analysis techniques will generate a contrast transfer coefficient (K^{trans}). This is variably described as an indicator of either capillary permeability or blood flow. In practice, the properties of the K^{trans} depend on the pharmacokinetic model used to calculate it. Measurements from a simple two-compartment model will be affected by blood volume (v_p), blood flow (F) and permeability surface area product (PS). The most commonly used models explicitly derive v_p such that K^{trans} represents the combined effects of F and PS. Measurements from the more complex adiabatic tissue homogeneity model [51] will separately calculate values for F so that K^{trans} represents the permeability surface area product of the capillary endothelium. However, these more complex analytical models are subject to greater fitting errors and are more sensitive to signal to noise ratio. The choice of appropriate model is guided by the requirements of the individual study with regard to the limitations of the available acquisition and post-processing hardware and expertise [52].

Flow

Perfusion is the delivery of nutrient arterial blood to the tissue capillary bed under steady-state conditions, and is the key aspect of microvascular function. Defined

in a neuroimaging context as cerebral blood flow (CBF), this physiological property can be examined by looking at a number of related physical parameters and their imaging correlates. Techniques that utilise a freely diffusible tracer, specifically $H_2{}^{15}O$ PET and xenon-enhanced CT, quantify transfer of tracer from the vascular to the extravascular compartment and therefore accurately reflect perfusion. The term perfusion is commonly applied to techniques that actually measure some other aspect of blood flow, which is not strictly accurate, since tissues contain vessels in which the blood flow is not directly contributing to tissue nutrition and therefore perfusion. This occurs when arterial branches traversing the region of interest (ROI) feed a separate capillary bed.

While sometimes referred to using an umbrella term of perfusion-weighted imaging (PWI), approximations of true flow may be calculated from DSC-MRI, DCE-MRI or DCE-CT, $H_2{}^{15}O$ PET, xenon-CT and arterial spin labelling (ASL). The last three techniques are designed specifically to measure capillary perfusion. DSC-MRI is purported to measure capillary perfusion due to the relative amplification of signal from areas with a low CBV, such as cerebral capillary beds, which occurs because of the susceptibility effect in T_2* imaging. In practice, flow measurements are based on a number of assumptions concerning the speed of contrast delivery and the identification of an appropriate arterial input function (AIF), *i.e.* the change in tracer concentration over time in the feeding vessel (Figure 3). In normal tissue these assumptions are more appropriate but in tumour tissue, where the nature and timing of the AIF cannot be assessed, the use of DSC-MRI to derive absolute flow measurements may be considered inappropriate [53–55]. DCE-MRI can, as mentioned previously, be analysed using a complex pharmacokinetic model which considers capillary transit to produce estimates of flow but demands almost prohibitively high temporal resolution and signal-to-noise ratio in the data, and therefore this technique has not been widely used [51].

Vessel size imaging

Information about the morphology of tumour microvasculature can be derived from first-pass and steady-state techniques employing gadolinium contrast agents and ultrasmall superparamagnetic iron oxide (USPIO) respectively. These techniques, known as vessel size imaging (VSI), can produce absolute quantitative measures of average vessel size (*R*v) and absolute measures of CBF [56], and can be used to determine fractional blood volume (fBV), which has been correlated with tumour blood volume from tracer studies [57]. They have also been validated against histology in animal glioma models [58].

Relative recirculation

Following the change in signal or concentration over time in dynamic imaging reveals that the curve does not return to baseline following the first pass of the tracer bolus (Figure 3). While gamma-variate fitting removes this discrepancy for the purposes of first-pass analysis, useful information has been derived from this phenomenon, which is related to a delay in circulation of the tracer through areas of the tumour vasculature with low perfusion pressure. This has been described by different sources as percentage recovery (100% representing complete recovery to baseline) or relative recirculation (rR), and may reflect local vascular tortuosity and lack of autoregulatory control [59].

Other techniques

Imaging of these microvascular parameters in brain tumours under physiological challenge with vasomodulator drugs, or gases such as carbogen, are unlikely to gain widespread use owing to the clinical challenges in potentially unwell patients. Utilising inspired oxygen as a contrast agent to alter the relaxivity of blood and tissues is currently under investigation as an MR proxy for vascular function and oxygen delivery in a variety of tumours [160]. It is hoped this will have potential as an MR technique to complement information from hypoxia measures such as ^{18}FMISO PET and this is preferred owing to the less problematic use of oxygen in the clinical setting. Alternative techniques that employ combinations of ASL sequences and blood oxygen level dependent (BOLD) sequences as used in functional MRI can be used to determine maps of cerebral metabolic rate of oxygen use ($CMRO_2$) in addition to measures of permeability. However, these techniques are at an early stage of development.

Applications of vascular biomarkers in cerebral malignancy

Neoplasm and its differential diagnosis

Imaging biomarkers of the vascular microenvironment, whose development has been driven largely by tumour research, have been utilised to improve radiological diagnostic performance, particularly for solitary, ring-enhancing lesions, and in the distinction of surgical from non-surgical lesions. Prospective clinical trials are necessary to define the sensitivity, specificity and predictive values of these biomarkers in clinical use and, in particular, methodological questions regarding the repeatability and reproducibility of parametric measurements within and between centres have still to be fully addressed.

Distinguishing solitary metastasis from glioma

Discriminating HGG from solitary enhancing cerebral metastases can be difficult, but it is an important distinction in determining the need for surgical intervention. Signal peak height and the degree of signal recovery using DSC-MRI have shown value in differentiating between the two [60]. In malignant glioma, rCBV values were found to be higher than in metastasis, particularly measurements from the region surrounding the enhancing tumour. This has been attributed to mixed vasogenic and cytotoxic oedema (due to tumour infiltrating along white matter tracts) in glioma compared with predominantly vasogenic oedema surrounding metastases [61]. ASL studies have detected similar patterns with significantly higher CBF in the T_2 weighted high signal areas surrounding GBM than surrounding metastases. Further large prospective studies are required, however, before such findings can be reliably applied to clinical practice. Kremer et al used DSC-MRI to compare

the mean rCBV in HGG and solitary cerebral metastasis in patients with melanoma, renal and lung carcinoma. Higher values were found in melanoma and renal metastases, although lower values in HGG were indistinguishable from lung metastases [62].

Distinguishing lymphoma from glioma

Since resection of primary cerebral lymphoma can worsen prognosis and result in unnecessary and avoidable patient morbidity, non-invasive diagnosis is preferred [63]. Malignant glioma is known to rely much more heavily upon a network of new blood vessels than malignant lymphoma. This difference has been exploited in order to differentiate the two based on the far higher rCBV values seen in HGG (Figure 4) [64–66]. Semi-quantitative evaluation of the signal–intensity time curve also revealed patterns characteristic of primary lymphoma [67]. Maximum rCBV has not only been found to be significantly lower in lymphomas than gliomas, but this was also reflected in a lower MVD on immunohistochemical examination [68]. In addition, HGG has been shown to have higher blood flow than lymphoma using ASL. Figure 4 shows an example of the relative blood volumes from DSC-MRI in lymphoma *vs* HGG.

Characterising meningioma

Although extra-axial in location, meningiomas are the most common primary intracranial neoplasm. Using DSC-MRI, extra-axial tumours have been shown to generally exhibit higher rCBV values than enhancing intra-axial tumours [69], although to be related to their extra-axial location and vascular origin, although meningiomas also have higher rCBV values than either schwannomas or neurinomas [70, 71]. Meningiomas are vascular tumours with potential for morbidity related to intra-operative bleeding. At low field strength (0.23 T), time to peak (TTP) from DCE-MRI was associated with MVD in meningioma, although the risk of surgical bleeding was more highly associated with conventional MR [72]. More recent reports have suggested that DSC-MRI can detect increased permeability in meningiomas with a partial internal carotid blood supply (via pial rather than dural vessels). This is thought to have implications to patient selection for pre-operative dural vessel embolisation and for planning resections of pial supplied tumours, which are more likely to bleed intra-operatively [73].

DCE-MRI has also been used to differentiate true intra-axial tumours from the subset of meningiomas that have imaging features resembling intra-axial tumours [74]. ASL has been used to determine blood flow in both meningiomas and gliomas [75–77]. Continuous (c)ASL-derived relative changes in signal intensity (%SI) time curves were also found to correlate with microvascular area as determined histologically by CD31 expression. In general, the values for the various perfusion metrics from each technique were higher in angiomatous meningioma than in fibrous meningioma. Similarly, K^{trans} has been shown to be helpful in distinguishing typical from atypical meningiomas that demonstrate similar rCBV values (Figure 5) [78].

Mixed tumour series

Other studies have examined the usefulness of perfusion imaging in mixed series of intracranial lesions. Noguchi et al [79] employed ASL in 35 patients with brain tumours and were able to distinguish haemangioblastomas from glioma, meningioma and schwannoma based on the maximal signal intensity within a tumour ROI normalised to ''normal'' white matter. They also reported a positive correlation between this measure and MVD on six histological subtypes of primary brain tumour. Additionally, there was a positive correlation between the percentage change in signal intensity (%SI) and MIB-1 (an antibody directed at proliferation antigen Ki-67 in gliomas), suggesting a link between proliferation and angiogenesis [79]. Weber et al [80] assessed conventional imaging and MRS against perfusion-weighted imaging (ASL, DSC-MRI and DCE-MRI) for the discrimination of GBM from metastases, lymphomas and other types of glioma. They concluded that perfusion-weighted imaging had the greatest predictive success, with GBM once again reporting the highest flow values. Receiver operating characteristic (ROC) analysis identified a threshold rCBF value of 1.4 with sensitivity 97%, specificity 50%, positive predictive value (PPV) 84% and negative predictive value (NPV) 86% for discriminating grade IV from grade III gliomas. This relatively low specificity remains problematic in separating grade IV and III gliomas using perfusion metrics. The sensitivity increased to 94% for discriminating grade IV from grade II (non-malignant) lesions. The higher blood flow in GBM also allowed differentiation from lymphoma, an rCBF cut-off of 1.2 possessing sensitivity, specificity, PPV and NPV of 97%, 80%, 94% and 89%, respectively. The authors recommended the use of PWI over MRS on commonplace 1.5 T clinical scanners due to the improved differential capability and shorter acquisition

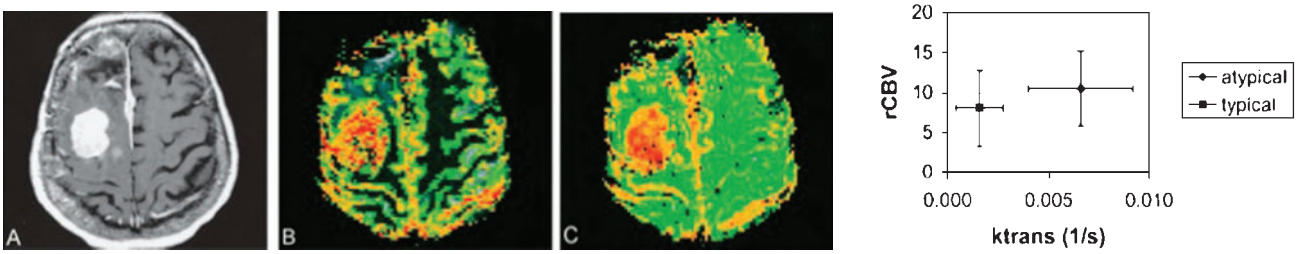

(a) (b)

Figure 5. (a) Images from a pathologically confirmed atypical meningioma: A, contrast-enhanced T_1; B, CBV (cerebral blood volume) overlay; C, permeability (reproduced with permission from [78]). (b) Scatter plot showing the range of values for rCBV and K^{trans} in typical and atypical meningioma.

times, and concluded the diagnostic power of ASL and DSC-MRI was comparable. While ASL benefits from the lack of exogenous intravenous contrast, DSC-MRI can be acquired more quickly, particularly at lower field strengths. As contrast is almost universally administered to tumour patients, DSC-MRI is gaining prevalence as a means of generating microvascular information during the injection that is otherwise ignored. Use of an extended pharmacokinetic model with two extravascular compartments and a measurement of blood volume allowed differentiation of glioma, metastasis and meningioma [81]. Additionally, a scatter plot of extravascular volume against blood volume differentiated between necrotising and proliferating tumour tissue, which may have usefulness in monitoring therapy.

Distinguishing infection from glioma

Abscess is one of the main differential diagnoses of GBM. While diffusion-weighted imaging is becoming routine for clinical diagnosis of abscess, studies have demonstrated significant separation between CBV values observed in abscesses *vs* cystic HGG (Figure 6) [82–84]. The mean rCBV from DSC-MRI in rim-enhancing lesions was found to be higher in cystic high-grade neoplasm than in cerebral abscesses [83]. Specificity increased if perfusion data were combined with measurements of the apparent diffusion coefficient (ADC), which was found to be higher in abscesses, possibly reflecting the reduction in cellularity caused by tissue destruction compared with new tissue formation in neoplasia [85, 86]. Haris et al [87] examined infective brain lesions, HGG and LGG with DCE-MRI comparing rCBV, rCBF, K^{trans} and v_e with VEGF expression and histopathological MVD. MVD was correlated with VEGF expression and rCBV, whereas K^{trans} was not. Although each parameter was significantly different among the three groups, the predictive value was not absolute. The DCE-MRI parameters of K^{trans} and v_e were recommended as adjuncts to differentiation of infective from surgical intracranial lesions on conventional imaging, rather than as replacements.

Distinguishing inflammation from glioma

Tumefactive demyelinating lesions (TDLs) as seen in multiple sclerosis (MS) can be difficult to differentiate from neoplasm on conventional MRI. The passage of large molecules across the BBB [88] and increased levels of VEGF in the CSF have been found in MS [89], indicating an inflammatory process that may share some of the pathophysiological steps associated with BTB disruption. Regional CBV derived by DSC-MRI has been shown to differentiate TDL from intracranial neoplasm, including primary lymphoma, with lower values seen in

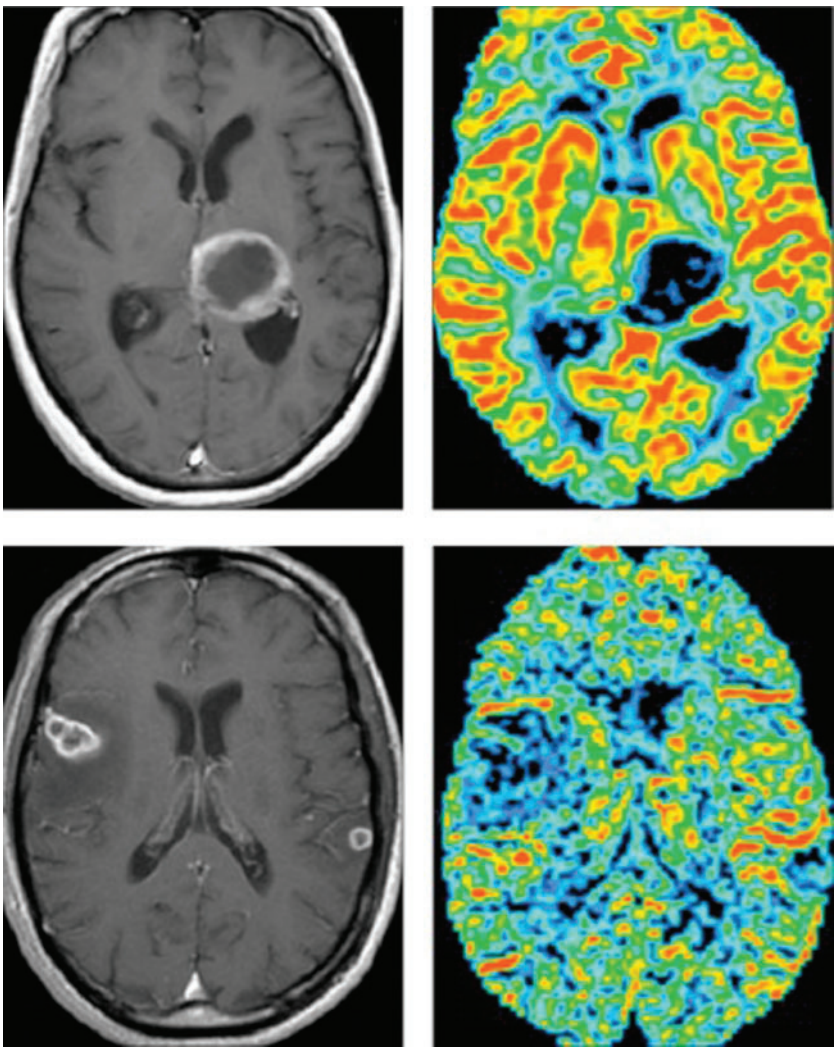

Figure 6. Post-contrast T_1 (left) and cerebral blood volume maps from a glioblastoma multiforme (top) and cerebral abscesses (bottom). (Reproduced from [83] with permission).

demyelination than in neoplasia [90]. Differentiation remains largely reliant on the clinical presentation.

Significance of microvascular properties in glioma

The *in vivo* analysis of tumour microvasculature aids: pre-operative grading of glioma; selection of representative biopsy sites; accurate determination of tumour extent; and monitoring of LGGs for potential malignant change. A number of studies have addressed the utility of imaging biomarkers of angiogenesis in these roles. Advanced imaging techniques have been mooted as key elements in the formulation of novel glial tumour classification systems that extend beyond the World Health Organization (WHO) histopathological classification and incorporate cytogenetic features, histopathological features and imaging features for the improvement of grading accuracy and predicting response to treatment [91].

Grading and histological subtype

Numerous studies have addressed the question of whether perfusion MRI, alone or in conjunction with other techniques, can accurately predict histopathological grade in glioma [84, 92, 93]. Early work utilising DSC-MRI with a first-pass, non-diffusible tracer model showed statistically higher rCBV in high-grade than in low-grade astrocytoma [94]. Subsequently there is an extensive body of work from the last decade showing a correlation of dynamic MRI parameters with WHO glioma grade, distinguishing LGG from HGG with good sensitivity and specificity [95].

In other studies, both K^{trans} and rCBV have been shown to be independently predictive of glioma grade with sensitivity and specificity greater than 90% [96]. Using DSC-MRI, rCBF was investigated in parallel to the related but more widely utilised parameter rCBV, and was found to be significantly higher in HGG and able to discriminate between grades independently [82]. A DSC-MRI study correlating a variety of pharmacokinetic models with histopathological grade found rCBV from a single compartment model, CBF and CBV from a single compartment model with automated AIF, and K^{trans} and v_p from a two-compartment model all correlated well. The optimal parametric combination was found to be K^{trans} and rCBV, with rCBV being the single best predictor of grade [97]. Warmuth et al [77] compared rCBV measurements from ASL and DSC-MRI and found them equally effective in distinguishing HGG from LGG, although ASL underestimated flow in areas with apparently lower flow rates. This reflects a known limitation of ASL for measurement of CBF in areas of lower flow such as white matter. These findings were reinforced by a later study using a combination of ^{1}H-MRS and perfusion imaging for the differentiation of HGG from LGG that found the metric with the single best performance in detecting malignancy in gliomas was the rCBV derived from DSC-MRI [98].

Traditional analysis employs ROI approaches to extract values from parametric maps. Histogram analysis of the distribution of normalised CBV values within the tumour ROI has been described as an alternative to the ''hot-spot'' (ROI maximum) method for differentiating tumours and provides more accurate differential diagnosis and better interobserver reproducibility in glioma [99]. Histogram techniques have the advantage of being more noise resistant than voxelwise maximum values. Young et al [100] employed a variety of analysis metrics to describe the shape of the histogram in tumoural, peritumoural and unsegmented tumoural regions within the CBF, CBV and rCBV maps in glioma. The peritumoural histogram metrics reportedly outperformed the standard methods and other histogram techniques in the determination of glioma grade, with rCBV again being the optimal studied parameter. Additionally, automated histogram analysis of whole-volume DSC-MRI has shown to be as effective as ROI analysis by an experienced observer when deriving rCBV for the grading of cerebral glioma, thereby eliminating the operator-dependent step of ROI selection [101].

Histogram analysis of rR showed a lower mean value in grade II gliomas, while the distribution of pixel rR values could discriminate between grade III and grade IV [59]. VASO imaging has also been shown to distinguish HGG from LGG, although differentiating grade III from grade IV was less robust [102].

Great interest has been placed in differentiating grade II oligodendrogial tumours from grade II astrocytomas, owing to the difference in behaviour and therapy. Cha et al [103] showed that $rCBV_{max}$ from DSC-MRI had significantly higher values in low-grade oligodendrogliomas than in astrocytomas (Figure 7). Several groups have confirmed the finding of high CBV values in oligodendroglial tumours [103, 104] that have ''chicken wire'' vasculature where the local rCBV can be as high as that of GBM.

Although less favoured than MR due to radiation considerations, perfusion CT has also been used to differentiate between LGG and HGG with similar sensitivity and specificity to standard clinical MRI [105]. This study found nCBV (normalised CBV) to be the single best metric with sensitivity 85.7% and specificity 100% with a cut-off of 1.92 compared with 85.7% and 60% for conventional MRI. Similarly, Jain et al [106] reported increased PS and CBV derived from perfusion CT correlated with tumour grade, and PS in particular could discern grade III from grade IV neoplasms, a diagnostic feature many perfusion MR studies have failed to demonstrate. CT techniques may have a role in situations where MR is contraindicated, but where advanced characterisation of lesions is desirable.

The use of DSC-MRI obtained during routine clinical examination and analysed with vendor-supplied software, which is of particular relevance to current clinical practice, has shown that rCBV had greater utility in the grading of glioma (HGG *vs* LGG) than in the differentiation of solitary metastases from HGG [107]. This work reported rCBV thresholds of 3.9 for solid tumour and 1.9 for peritumoural oedema and described high sensitivity, specificity and accuracy in the differentiation of HGG from LGG. High rCBV in the peritumoural ''oedema'' of HGG contrasted with an rCBV of approximately 1.0 in metastases.

Tumour genetic status

Genetic factors such as loss of heterozygosity (LOH) of chromosomes 1p/19q have been shown to be important

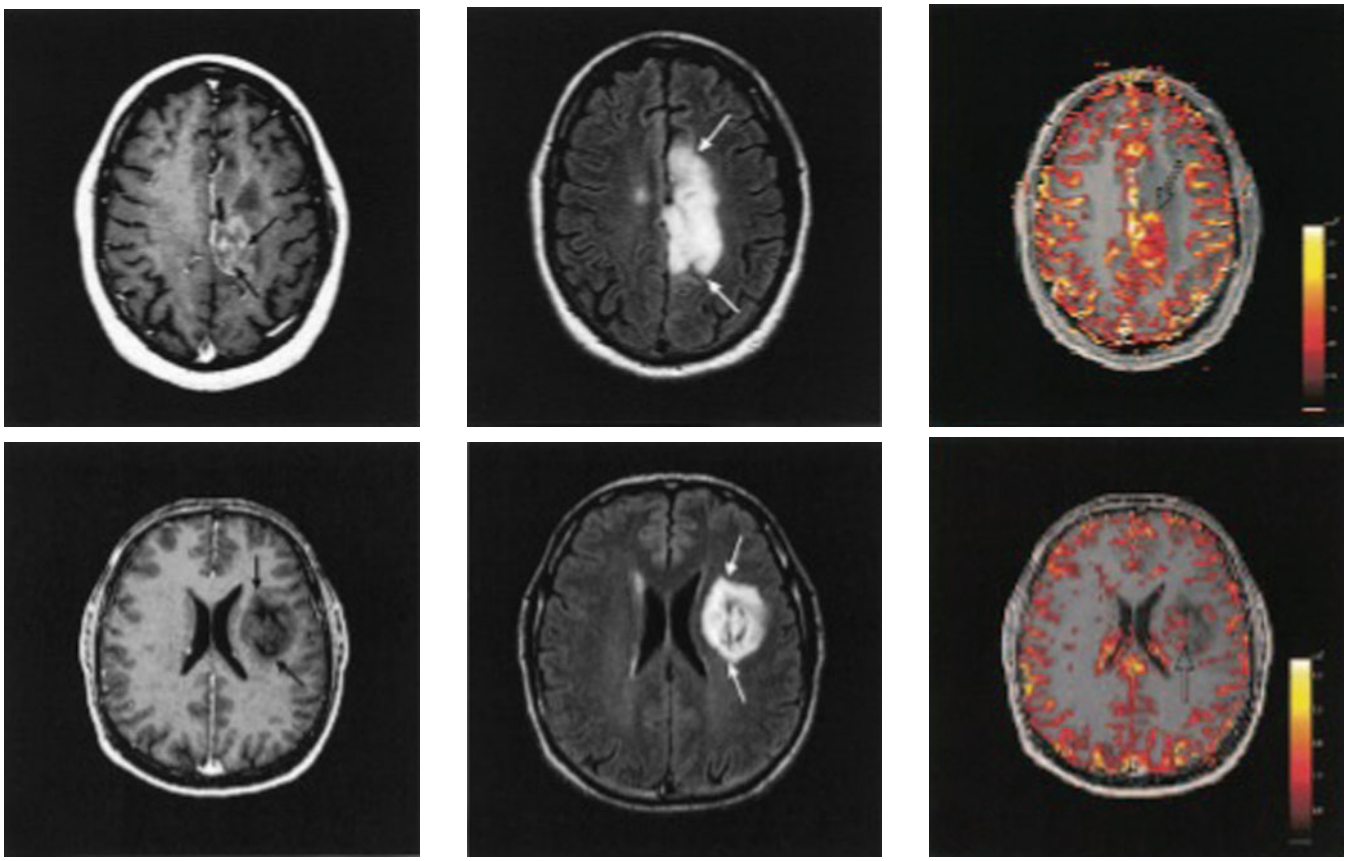

Figure 7. (a) Post-contrast T_1, (b) fluid-attenuated inversion-recovery (FLAIR) and (c) cerebral blood volume (CBV) maps from in patients with an oligodendrocytoma (top) and an astrocytoma (bottom) (reproduced from [103] with permission).

biomarkers of chemosensitivity in gliomas [108] (Figure 8). Jenkinson et al [109] found higher rCBV levels in oligodendroglial tumours exhibiting the –1p/–19q genotype than those with no LOH. Law et al [110] subsequently found increased rCBV values in gliomas with 1p deletions compared with those without. In contrast, deletions of 19q—in isolation or with coexistent 1p deletions—produced no increase in rCBV. They proposed a diagnostic protocol for the molecular typing of gliomas with high rCBV suggestive of 1p deletion.

Emblem et al [99], recognising the confounding effect that high blood volume benign oligodendroglial tumours can have on non-invasive glioma grading methodologies, assessed the histograms of rCBV values in glioma. They reported that the normalised peak height of the histograms could differentiate low-grade oligodendroglial tumours with maintained 1p/19q heterozygosity from other gliomas with 100% sensitivity and 91% specificity. The technique was also used to distinguish LGG from HGG as previously discussed.

Tumour edge and extent

Conventional imaging appearances of the tumour often guide the ROI and histogram analysis and thus much spatial information, particularly in the region surrounding the contrast-enhancing tumour, is discarded. This tissue is likely to contain invasive malignant cells not observed by standard imaging. Although diffusion-weighted imaging (DWI) is the main methodology for examining microscopic tumour extension by evaluating changes in cellular density, extracellular matrix and white matter tract integrity, metabolic and perfusion imaging have also been used. Glioma extension beyond the visible edge on conventional imaging has been detected with methionine PET and been correlated with CBV and histology suggestive of focal malignancy [40]. Metabolic PET is being considered as a tool to guide surgical and radiotherapy planning, and the more accessible parametric maps produced by DSC-MRI may be useful in this regard [111–113]. Di Costanzo et al [114] utilised a combination of spectroscopy, DWI and rCBV from PWI at 3 T in 31 patients with glioma (21 HGG, 10 LGG) and concluded the combination of all 3 could discriminate invasive tumour from surrounding oedema or unaffected brain tissue, and could discriminate HGG from LGG. Assessment was carried out using small ROIs in the tissue of interest with normalisation to contralateral tissue. The HGG rCBV values were 3.70 ± 1.06 in the tumour mass and 3.39 ± 1.00 in the margin. Lower values were detected in peritumoural tissues, with rCBV <1.0 in largely oedematous tissue, increasing with some invasive tumour burden to 1.68 ± 0.41. Values in the bulk or margin of LGGs could not be confidently distinguished from contralateral tissue [114].

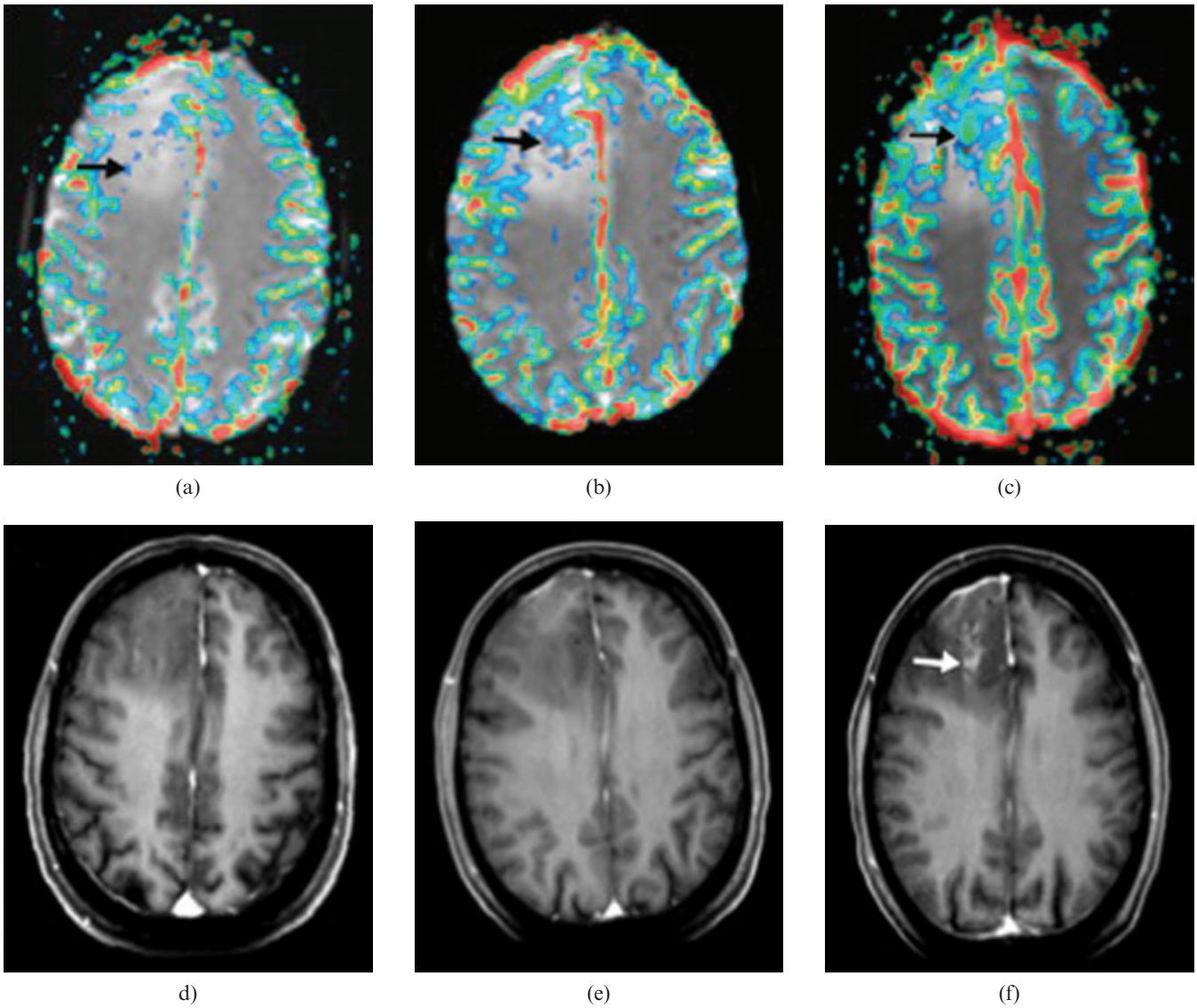

Figure 8. Images from serial MR perfusion studies in 30-year-old patient with oligodendroglioma that showed progression to high-grade tumour 18 months after study entry. (a–c) Transverse rCBV (relative cerebral blood volume) overlay images. (d–f) Transverse reformatted images obtained with double-dose contrast-enhanced volumetric T_1 weighted sequence (spoiled gradient echo; 14.4/6.4; inversion time, 650 ms). (a) rCBV map at baseline shows small area of elevated rCBV (arrow) measuring up to 4.52. (b) rCBV map 6 months before transformation shows larger area of increased rCBV (arrow) measuring up to 8.32. (c) rCBV map at transformation shows further increase in area with elevated rCBV (arrow), which now reaches a maximum value of 12.04. (d) Baseline contrast-enhanced T_1 weighted image shows a hypointense tumour without pathological enhancement. (e) Six months before transformation, there is no evidence of pathological intratumoural enhancement, despite a markedly increased rCBV. (f) At transformation, there is irregular enhancement in centre of the tumour (arrow); the area of pathological enhancement is much smaller than the region of increased rCBV (reproduced from [115] with permission).

Prognosis and transformation

LGG have a propensity to undergo malignant transformation and become HGG although the timescale is highly variable between individuals. A study of prospective serial DSC-MRI in LGG investigating the relationship between rCBV and malignant transformation found no significant difference in rCBV between malignant transformers and non-transformers at baseline. However, the rCBV at 12 months and 6 months prior to eventual transformation were significantly greater in transforming than in non-transforming gliomas; suggesting rCBV measurement in LGG may allow prediction of malignant transformation with up to a 1 year lead time compared with contrast-enhanced T_1 weighted imaging (Figure 8) [115]. During follow-up of both HGGs and LGGs, Siegel et al [116] reported on the clinical utility of rCBV in detecting increasing grade and progression earlier than MRI, SPECT and clinical assessment in up to two-thirds of patients with a mean lead time of between 4.5 and 6 months. They also described the usefulness of rCBV in differentiating tumour necrosis and non-tumoural enhancing lesions from infiltrative recurrence. Law's group have employed DSC-MRI to identify subsets of LGGs (astrocytomas, oligodendrogliomas and oligoastrocytomas), which progressed rapidly or were more likely to undergo malignant change [117]. They determined an rCBV cut-off of

1.75, above which LGG exhibited significantly shorter time to progression (4620 days *vs* 245 days). They later demonstrated that LGG with rCBV >1.75 on DSC-MRI had a significantly shorter median time to progression (265 days *vs* 3585 days) regardless of pathological findings. Relative CBV was also an independent predictor of prognosis in this cohort [118].

In a follow-up study of 41 malignant glioma patients enrolled in a Phase II temozolomide trial, imaging 3–4 weeks after chemoradiotherapy and every 2 months thereafter, failed to show a benefit from PWI or DWI in predicting response as defined by conventional imaging criteria [119]. Such approaches can be problematic since conventional imaging may be misleading as a *de facto* description of therapeutic response. In a study of a first-pass pharmacokinetic model of DCE-MRI in glioma, both K^{trans} and CBV were shown to correlate with tumour grade [120]. Furthermore, WHO grade, K^{trans} and CBV were all directly correlated with survival, although Cox's regression analysis identified only grade and K^{trans} as significant independent prognostic factors [121]. K^{trans} exhibited a direct relationship with survival in grade IV gliomas (Figure 9). This initially appears counterintuitive as more aggressive tumours should have higher angiogenesis rates and hence leakier vessels; however, it most likely reflects better drug delivery and potentially greater therapeutic sensitivity in patients with higher K^{trans} values [121].

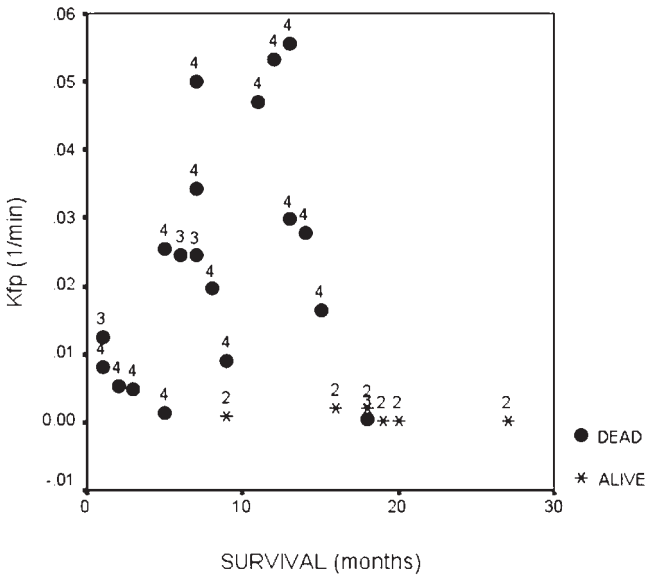

Figure 9. Scatter plot showing survival in patients with high grade and low-grade glioma compared to measured K^{trans} (extracted from first-pass analysis and termed Kfp). The figure shows a clear relationship between survival and K^{trans} in high-grade glioma.

Progression vs *treatment effects*

Progression vs *pseudoprogression*

Radiotherapy has been the foundation of GBM management for over 30 years. Radiation-related treatment effects are classified as acute (occurring during therapy), sub-acute (in the 12 weeks following irradiation) or late (occurring after 3 months from cessation of treatment). An increase in the contrast-enhancing region on conventional MR during the early post-irradiation period, which subsequently resolves without intervention, has been described [122]. This appearance mimics that seen in tumour progression in the initial stages and is referred to as pseudoprogression. Routinely employed MRI sequences are unable to distinguish accurately between true progression and early or late treatment-related effects. The distinction between true progression and treatment-related effects is crucial in the management decision-making process, since one represents treatment failure while the other may actually be related to treatment sensitivity.

The incidence of pseudoprogression has been reported as 9% (3/32) for radiation alone and 21% (18/85) to 31% (32/103) with concomitant temozolomide [123–125]. Oedema and conventional contrast enhancement resulting from leaky neoangiogenic vessels in progressive HGG cannot be distinguished from that caused by temozolomide chemoradiotherapy in responsive patients with pseudoprogression. Therefore, the ability to image angiogenesis and tumour microvasculature has been hypothesised to improve the sensitivity and specificity of this important clinical distinction. In addition, the confounding effect which pseudoprogression can have on early detection of disease progression by current standard methods—contrast-enhanced T_1 weighted MRI with RECIST criteria—means that a different progression biomarker is required to assess response and potentially to allow early stratification of treatment. Angiogenesis biomarkers could provide greater information regarding the microvascular changes which take place during pseudoprogression.

Recurrence vs *radiation necrosis*

Radiation necrosis is a severe non-neoplastic tissue injury, generally occurring between 4 and 12 months post-radiation. It is related to the areas of highest radiation dose. In one study 51% (26/51) of patients exhibited radiological evidence of glioma progression within 6 months of temozolomide radiotherapy. 15 of the 26 patients were managed surgically, with almost half of those ($n = 7$) found to have radiation necrosis with no evidence of recurrence [126]. Dual isotope SPECT with thallium-201 and the perfusion agent ^{99m}Tc-HMPAO have shown potential in separating tumour recurrence from non-specific changes in symptomatic, post-radiotherapy glioblastoma patients, matching 14 of the 15 histopathological samples [127]. In a small Phase II trial of thalidomide and radiotherapy in paediatric brain stem gliomas and GBM, advanced imaging techniques such as FDG-PET, PWI and MRS aided the distinction of recurrence from treatment effect [128]. DCE-MRI follow-up of patients with a variety of cerebral tumours who developed small enhancing lesions in the radiotherapy field following treatment showed relative CBV values were lower in non-neoplastic enhancement (rCBV <0.6) than in recurrence (rCBV>2.6), but the inability to robustly discriminate between the values was a major drawback [129].

While DWI, MRS and FDG-PET have been investigated as methods for the differential diagnosis of radiation injury from progression [130–135], the specificity is not currently sufficient, and other modalities and

combinations must be investigated. Perfusion CT (analysed using commercial software) has shown that recurrent tumours exhibit lower normalised (n)MTT (normalised mean transit time) and higher nCBV and nCBF than radiation necrosis [136]. The sensitivities and specificities of nCBV with a cut-off value of 1.65 were 83.3% and 100%, for nCBF with a threshold of 1.28 they were 94.4% and 87.5%, whereas in nMTT they were 94.4% and 75% with a threshold of 1.44. Hu et al [137] attempted to establish DSC-MRI rCBV thresholds to differentiate post-treatment radiation effects from tumour recurrence in 13 volunteers using both T_1 and T_2 leakage-corrected techniques that were correlated with biopsy location. An rCBV threshold value of 0.71 was reported with a sensitivity of 91.7% and a specificity of 100% for distinguishing post-treatment radiation effects from recurrent disease. The overall evidence supports the notion that radiation necrosis exhibits lower rCBV owing to transient leakiness rather than new vessel formation or significant changes in vessel calibre.

Therapeutic response

Radiotherapy and chemotherapy

Cao et al [138] analysed data from glioma patients undergoing radiotherapy by classifying the tumours into regions of low and high blood volume on DSC-MRI. Through proportional hazards survival analysis, they demonstrated that the group of patients with tumours comprising lower proportions of high rCBV (<7% of the fluid-attenuated inversion-recovery (FLAIR) abnormality) pre-treatment exhibited a statistically significant increase in overall survival. In addition, a decrease in the fraction of low rCBV at week 1 post radiotherapy was associated with better survival, as was a decrease in the fractional high rCBV at week 3. They suggested vascular tumours are more aggressive, and that increased CBV during week 1, followed by a decrease in week 3, is the trajectory of rCBV change indicative of tumours responding to radiotherapy [138]. This indicates the potential to delineate areas within tumours with differential radiosensitivity, which may benefit from boost and highly conformal radiotherapy techniques. Similarly, following surgical resection of cerebral metastases, rCBV measured at 6 weeks post-operatively was predictive of overall outcome with a sensitivity of 90% compared with 64% for volume change alone [139].

Response to radiotherapy is important not only in the context of the tumour and the timing of concomitant chemotherapy, but has prognostic implications for the damage to adjacent eloquent white matter. Lee et al [140] detected a decrease in the rCBV peak height and an increase in rR using DSC-MRI in normal appearing white matter in a dose-dependent manner in the radiotherapy field. They concluded that these changes reflected a decrease in vessel density with a concomitant increase in tortuosity or permeability in the 2 months following radiotherapy. Fuss et al [141] examined rCBV in grade II astrocytomas and the surrounding grey and white matter following conformal radiotherapy, observing a significant fall in rCBV in normal brain exposed to >40% of the dose, but not in areas receiving lower doses. They also documented radiation-induced changes in rCBV in the tumours themselves despite a lack of response on conventional MRI. In a small group of patients undergoing conformal radiotherapy, Price et al [142] reported no changes in rCBF and rCBV outside the 60% isodose line (32 Gy) during follow up, with a dose-related decrease in both parameters in normal brain at higher doses. These findings have the potential to predict collateral changes during radiotherapy, although further work is required to determine thresholds for the utility of perfusion MR in detecting subclinical radiation changes in normal brain during radiotherapy. As survival improves with the advent of new therapies, the issue of collateral radiation damage in eloquent brain may become increasingly clinically relevant.

Since concomitant and adjuvant temozolomide chemoradiotherapy is now the current standard of care in GBM, there is interest in the potential effects which timing of irradiation can have on the efficacy of chemotherapy. DCE-MRI studies have shown conformal radiotherapy has a greater impact on the permeability of BTB than of BBB, suggesting a preferential window for intravenous chemotherapy delivery from 1 week post initiation to 1 month post completion of radiotherapy [143]. More evidence for the usefulness of microvascular imaging may be derived once data are obtained on the administration of these agents during the proposed therapeutic window.

Corticosteroids are the first-line medical therapy in patients presenting with neurological effects secondary to peritumoural oedema and mass effect. Early evidence from xenon-CT demonstrated the rCBF in peritumoural oedema was significantly lower than contralateral white matter in glioma patients, and that this was not improved by dexamethasone therapy [144]. By contrast, Bastin et al [145] used DSC-MRI to evaluate the effects of dexamethasone and found no changes in CBV, CBF or MTT within enhancing tumour or normal appearing white matter following 2–3 days of dexamethasone 16 mg day^{-1}, but did report increases in rCBF in surrounding oedema. The authors suggested this was due to the reduction in tissue fluid reducing interstitial pressure and restoring flow. At present perfusion-weighted imaging techniques such as DSC-MRI have shown little value in predicting or detecting response to temozolomide in glioma [119]. However, a case report has noted areas of high rCBV corresponding to tumour volume reduction following chemotherapy with PCV [procarbazine, lomustine (CCNU) and vincristine], whereas areas of lower rCBV remained unchanged [146].

Emerging therapies

Considerable interest has arisen in targeted therapies directed against the angiogenic process or neo-angiogenic tumour vasculature [147–150]. These include the anti-VEGF antibody bevacizumab (avastin, Genentech, San Francisco, CA) that has shown improved progression-free survival [151] in a Phase II clinical trial of recurrent malignant glioma treated with bevacizumab and irinotecan in combination therapy. Objective disease response was correlated with VEGF expression [152]. Trials to validate these results in larger patient numbers, and to test bevacizumab alone in both recurrent and newly diagnosed disease, are under way. Similar

successes have also been seen in drugs that target VEGF and other growth factor receptor tyrosine kinases, so called tyrosine kinases inhibitors (TKIs) in extracranial solid tumours [150]. There are more than 60 Phase I/II trials of such therapies in malignant glioma completed or under way, and several imaging biomarkers have been used in analysis of these potential new treatments. Administration of a monoclonal antibody against VEGF in a rodent model of glioma produced a profound decrease in permeability as measured by DCE-MRI [153]. DCE-MRI was seen as a valuable adjunct to conventional imaging in a study assessing response to anti-angiogenic therapy with carboplatin and thalidomide, where rCBV correlated better than conventional measures with clinical status and response to therapy [154].

In a multicentre Phase I trial of an angiogenesis inhibitor, DSC-MRI revealed decreases in blood volume and blood flow in malignant glioma patients with a clinical response, demonstrating the potential for detecting alterations in perfusion parameters as markers of therapeutic response in humans [155]. Similarly, in a multicentre Phase I maximum tolerated dose study of cilengitide in recurrent malignant glioma, rCBF changes on PWI were significant following 16 weeks of treatment and were apparently related to treatment response as defined by conventional imaging [156]. Batchelor et al [157] used a number of MR parameters in the assessment of the oral anti-angiogenic pan-VEGFR tyrosine kinase inhibitors AZD2171 and noted reductions in vessel size and K^{trans}. K^{trans} may have decreased because of lower vascular surface area; however, it remained low even after vessel size increased, implying a reciprocal lowering of vascular permeability. The reversible nature of vascular normalisation (reduction in size and permeability) indicates the need for longitudinal monitoring of such therapies through non-invasive means such as DCE-MRI. By transiently reducing permeability, the size of the enhancing tumour on conventional imaging can shrink in the presence of unchanged or progressing underlying tumour bulk. This phenomenon—referred to as pseudoresponse—indicates the need for microvascular imaging with such treatments, but also highlights the utility of complementary advanced tumour imaging techniques. Imaging biomarkers of microvascaulture will have a key role in stratifying patients for anti-angiogenic therapy, and detecting response or therapeutic escape.

Conclusion

To date, there has been extensive use of advanced imaging techniques to grade and genetically type glioma, target tumours for biopsy and aid differential diagnosis. It is highly likely DSC-MRI, DCE-MRI and other imaging techniques will be applied increasingly to studies of novel and conventional therapeutic agents, particularly those targeted at tumour microvasculature. For all of these applications, variations in technique, the pros and cons of the modality and kinetic analysis employed, and the interpretation of the various derived parameters must be carefully considered before any links to biological outcomes are inferred. Further research is required to improve the acquisition, analysis and standardisation of data before widespread clinical use is feasible. It is likely, however, that standardised vascular imaging approaches will be combined with circulating biomarkers and complementary advanced imaging methodologies. With ongoing improvements in scanner hardware and post-processing techniques, these combined advanced approaches should be transferrable to the clinic. Ultimately, biomarkers of the tumour microvasculature will result in more specific and sensitive neuro-oncological diagnoses, more efficient clinical trial design and improved rationalisation of individualised cancer therapies. It is incumbent on those responsible for assessing novel imaging diagnostic and response criteria to be aware of the background surrounding their implementation and utility.

References

1. Stupp R, Mason WP, van den Bent MJ, et al. Radiotherapy plus concomitant and adjuvant temozolomide for glioblastoma. N Engl J Med 2005;352:987–96.
2. Brem S, Cotran R, Folkman J. Tumor angiogenesis: a quantitative method for histologic grading. J Natl Cancer Inst 1972;48:347–56.
3. Brem SS, Cotran RS, Folkman MJ. Angiogenesis in brain tumors: a quantitative histologic study. Surg Forum 1974;25: 462–4.
4. Wesseling P, van der Laak JA, H de Leeuw, et al. Computer-assisted analysis of the microvasculature in untreated glioblastomas. J Neurooncol 1995;24:83–5.
5. Cheng SY, Huang HJ, Nagane M, et al. Suppression of glioblastoma angiogenicity and tumorigenicity by inhibition of endogenous expression of vascular endothelial growth factor. Proc Natl Acad Sci U S A 1996;93:8502–7.
6. Brat DJ, Van Meir EG. Glomeruloid microvascular proliferation orchestrated by VPF/VEGF: a new world of angiogenesis research. Am J Pathol 2001;158:789–96.
7. Vajkoczy P, Menger MD. Vascular microenvironment in gliomas. J Neurooncol 2000;50:99–108.
8. Kargiotis O, Rao JS, Kyritsis AP. Mechanisms of angiogenesis in gliomas. J Neurooncol 2006;78:281–93.
9. Dunn IF, Heese O, Black PM. Growth factors in glioma angiogenesis: FGFs, PDGF, EGF, and TGFs. J Neurooncol 2000;50:121–37.
10. Machein MR, Plate KH. VEGF in brain tumors. J Neurooncol 2000;50:109–20.
11. Dvorak HF, Nagy JA, Feng D, et al. Vascular permeability factor/vascular endothelial growth factor and the significance of microvascular hyperpermeability in angiogenesis. Curr Top Microbiol Immunol 1999;237:97–132.
12. Senger DR, Van de Water L, Brown LF, et al. Vascular permeability factor (VPF, VEGF) in tumor biology. Cancer Metastasis Rev 1993;12:303–24.
13. Ashrafpour H, Huang N, Neligan PC, et al. Vasodilator effect and mechanism of action of vascular endothelial growth factor in skin vasculature. Am J Physiol Heart Circ Physiol 2004;286:H946–54.
14. Ku DD, Zaleski JK, Liu S, et al. Vascular endothelial growth factor induces EDRF-dependent relaxation in coronary arteries. Am J Physiol 1993;265:H586–92.
15. Wei W, Chen ZW, Yang Q, et al. Vasorelaxation induced by vascular endothelial growth factor in the human internal mammary artery and radial artery. Vascul Pharmacol 2007;46:253–9.
16. Senger DR, Galli SJ, Dvorak AM, et al. Tumor cells secrete a vascular permeability factor that promotes accumulation of ascites fluid. Science 1983;219:983–5.
17. Plate KH, Breier G, Weich HA, et al. Vascular endothelial growth factor is a potential tumour angiogenesis factor in human gliomas in vivo. Nature 1992;359:845–8.

18. Erdamar S, Bagci P, Oz B, et al. Correlation of endothelial nitric oxide synthase and vascular endothelial growth factor expression with malignancy in patients with astrocytic tumors. J Buon 2006;11:213–16.
19. Forsythe JA, Jiang BH, Iyer NV, et al. Activation of vascular endothelial growth factor gene transcription by hypoxia-inducible factor 1. Mol Cell Biol 1996;16:4604–13.
20. Kaur B, Khwaja FW, Severson EA, et al. Hypoxia and the hypoxia-inducible-factor pathway in glioma growth and angiogenesis. Neuro-oncol 2005;7:134–53.
21. Carlson MR, Pope WB, Horvath S, et al. Relationship between survival and edema in malignant gliomas: role of vascular endothelial growth factor and neuronal pentraxin 2. Clin Cancer Res 2007;13:2592–8.
22. Maiuri F, Del Basso De Caro ML, Iaconetta G, et al. Prognostic and survival-related factors in patients with well-differentiated oligodendrogliomas. Zentralbl Neurochir 2006;67:204–9.
23. Zhou YH, Hess KR, Liu L, et al. Modeling prognosis for patients with malignant astrocytic gliomas: quantifying the expression of multiple genetic markers and clinical variables. Neuro Oncol 2005;7:485–94.
24. Zhou YH, Tan F, Hess KR, et al. The expression of PAX6, PTEN, vascular endothelial growth factor, and epidermal growth factor receptor in gliomas: relationship to tumor grade and survival. Clin Cancer Res 2003;9:3369–75.
25. Vick NA, Bigner DD. Microvascular abnormalities in virally-induced canine brain tumors. Structural bases for altered blood-brain barrier function. J Neurol Sci 1972;17: 29–39.
26. Waggener JD, Beggs JL. Vasculature of Neural Neoplasms. Adv Neurol 1976;15:27–49.
27. Hansen S, Grabau DA, Rose C, et al. Angiogenesis in breast cancer: a comparative study of the observer variability of methods for determining microvessel density. Lab Invest 1998;78:1563–73.
28. Hansen S, Sorensen FB, Vach W, et al. Microvessel density compared with the Chalkley count in a prognostic study of angiogenesis in breast cancer patients. Histopathology 2004;44:428–36.
29. Blasberg RG, Kobayashi T, Horowitz M, et al. Regional blood flow in ethylnitrosourea-induced brain tumors. Ann Neurol 1983;14:189–201.
30. Groothuis DR, Pasternak JF, Fischer JM, et al. Regional measurements of blood flow in experimental RG-2 rat gliomas. Cancer Res 1983;43:3362–7.
31. Vajkoczy P, Schilling L, Ullrich A, et al. Characterization of angiogenesis and microcirculation of high-grade glioma: an intravital multifluorescence microscopic approach in the athymic nude mouse. J Cereb Blood Flow Metab 1998;18: 510–20.
32. Dellian M, Witwer BP, Salehi HA, et al. Quantitation and physiological characterization of angiogenic vessels in mice: effect of basic fibroblast growth factor, vascular endothelial growth factor/vascular permeability factor, and host microenvironment. Am J Pathol 1996;149:59–71.
33. Yuan F, Salehi HA, Boucher Y, et al. Vascular permeability and microcirculation of gliomas and mammary carcinomas transplanted in rat and mouse cranial windows. Cancer Res 1994;54:4564–8.
34. Hardebo JE, Kahrstrom J, Salford LG. Lack of neural control and reactivity to vasoactive agents in malignant glioma arteries. J Neurosurg 1991;74:633–5.
35. Hatakeyama T, Kawai N, Nishiyama Y, et al. 11C-methionine (MET) and 18F-fluorothymidine (FLT) PET in patients with newly diagnosed glioma. Eur J Nucl Med Mol Imaging 2008;35:2009–17.
36. Bruehlmeier M, Roelcke U, Schubiger PA, et al. Assessment of hypoxia and perfusion in human brain tumors using PET with 18F-fluoromisonidazole and 15O-H2O. J Nucl Med 2004;45:1851–9.
37. Stadlbauer A, Prante O, Nimsky C, et al. Metabolic imaging of cerebral gliomas: spatial correlation of changes in O-(2-18F-fluoroethyl)-L-tyrosine PET and proton magnetic resonance spectroscopic imaging. J Nucl Med 2008;49:721–9.
38. Herholz K, Coope D, Jackson A. Metabolic and molecular imaging in neuro-oncology. Lancet Neurol 2007;6:711–24.
39. Kracht LW, Friese M, Herholz K, et al. Methyl-[11C]-l-methionine uptake as measured by positron emission tomography correlates to microvessel density in patients with glioma. Eur J Nucl Med Mol Imaging 2003;30:868–73.
40. Sadeghi N, Salmon I, Decaestecker C, et al. Stereotactic comparison among cerebral blood volume, methionine uptake, and histopathology in brain glioma. AJNR Am J Neuroradiol 2007;28:455–61.
41. Sadeghi N, Salmon I, Tang BN, et al. Correlation between dynamic susceptibility contrast perfusion MRI and methionine metabolism in brain gliomas: preliminary results. J Magn Reson Imaging 2006;24:989–94.
42. Sadeghi N, D'Haene N, Decaestecker C, et al. Apparent diffusion coefficient and cerebral blood volume in brain gliomas: relation to tumor cell density and tumor microvessel density based on stereotactic biopsies. AJNR Am J Neuroradiol 2008;29:476–82.
43. Aronen HJ, Pardo FS, Kennedy DN, et al. High microvascular blood volume is associated with high glucose uptake and tumor angiogenesis in human gliomas. Clin Cancer Res 2000;6:2189–200.
44. Wyss MT, Hofer S, Hefti M, et al. Spatial heterogeneity of low-grade gliomas at the capillary level: a PET study on tumor blood flow and amino acid uptake. J Nucl Med 2007;48:1047–52.
45. Cox D, Aoki T, Seki J, et al. The pharmacology of the integrins. Med Res Rev 1994;14:195–228.
46. O'Reilly MS, Boehm T, Shing Y, et al. Endostatin: an endogenous inhibitor of angiogenesis and tumor growth. Cell 1997;88:277–85.
47. Buckley DL. Uncertainty in the analysis of tracer kinetics using dynamic contrast-enhanced T_1-weighted MRI. Magn Reson Med 2002;47:601–6.
48. Haroon HA, Patankar TF, Zhu XP, et al. Comparison of cerebral blood volume maps generated from T_2* and T_1 weighted MRI data in intra-axial cerebral tumours. Br J Radiol 2007;80:161–8.
49. Lu H, Golay X, Pekar JJ, et al. Functional magnetic resonance imaging based on changes in vascular space occupancy. Magn Reson Med 2003;50:263–74.
50. Lu H, van Zijl PC, Hendrikse J, et al. Multiple acquisitions with global inversion cycling (MAGIC): a multislice technique for vascular-space-occupancy dependent fMRI. Magn Reson Med 2004;51:9–15.
51. St Lawrence KS, Lee TY. An adiabatic approximation to the tissue homogeneity model for water exchange in the brain: II. Experimental validation. J Cereb Blood Flow Metab 1998;18:1378–85.
52. Tofts PS, Brix G, Buckley DL, et al. Estimating kinetic parameters from dynamic contrast-enhanced T(1)-weighted MRI of a diffusible tracer: standardized quantities and symbols. J Magn Reson Imaging 1999;10:223–32.
53. Calamante F, Gadian DG, Connelly A. Delay and dispersion effects in dynamic susceptibility contrast MRI: simulations using singular value decomposition. Magn Reson Med 2000;44:466–73.
54. Ostergaard L, Hochberg FH, Rabinov JD, et al. Early changes measured by magnetic resonance imaging in cerebral blood flow, blood volume, and blood-brain barrier permeability following dexamethasone treatment in patients with brain tumors. J Neurosurg 1999;90:300–5.
55. Thacker NA, Scott ML, Jackson A. Can dynamic susceptibility contrast magnetic resonance imaging perfusion data

be analysed using a model based on directional flow? J Magn Reson Imaging 2003;17:241–55.
56. Kiselev VG, Strecker R, Ziyeh S, et al. Vessel size imaging in humans. Magn Reson Med 2005;53:553–63.
57. Howe FA, McPhail LD, Griffiths JR, et al. Vessel size index magnetic resonance imaging to monitor the effect of antivascular treatment in a rodent tumor model. Int J Radiat Oncol Biol Phys 2008;71:1470–6.
58. Valable S, Lemasson B, Farion R, et al. Assessment of blood volume, vessel size, and the expression of angiogenic factors in two rat glioma models: a longitudinal in vivo and ex vivo study. NMR Biomed 2008;21:1043–56.
59. Jackson A, Kassner A, Annesley-Williams D, et al. Abnormalities in the recirculation phase of contrast agent bolus passage in cerebral gliomas: comparison with relative blood volume and tumor grade. AJNR Am J Neuroradiol 2002;23:7–14.
60. Cha S, Lupo JM, Chen MH, et al. Differentiation of glioblastoma multiforme and single brain metastasis by peak height and percentage of signal intensity recovery derived from dynamic susceptibility-weighted contrast-enhanced perfusion MR imaging. AJNR Am J Neuroradiol 2007;28:1078–84.
61. Law M, Cha S, Knopp EA, et al. High-grade gliomas and solitary metastases: differentiation by using perfusion and proton spectroscopic MR imaging. Radiology 2002;222: 715–21.
62. Kremer S, Grand S, Berger F, et al. Dynamic contrast-enhanced MRI: differentiating melanoma and renal carcinoma metastases from high-grade astrocytomas and other metastases. Neuroradiology 2003;45:44–9.
63. Pollack IF, Lunsford LD, Flickinger JC, et al. Prognostic factors in the diagnosis and treatment of primary central nervous system lymphoma. Cancer 1989;63:939–47.
64. Sugahara T, Korogi Y, Shigematsu Y, et al. Perfusion-sensitive MRI of cerebral lymphomas: a preliminary report. J Comput Assist Tomogr 1999;23:232–7.
65. Cha S, Knopp EA, Johnson G, et al. Intracranial mass lesions: dynamic contrast-enhanced susceptibility-weighted echo-planar perfusion MR imaging. Radiology 2002;223:11–29.
66. Calli C, Kitis O, Yunten N, et al. Perfusion and diffusion MR imaging in enhancing malignant cerebral tumors. Eur J Radiol 2006;58:394–403.
67. Hartmann M, Heiland S, Harting I, et al. Distinguishing of primary cerebral lymphoma from high-grade glioma with perfusion-weighted magnetic resonance imaging. Neurosci Lett 2003;338:119–22.
68. Liao W, Liu Y, Wang X, et al. Differentiation of primary central nervous system lymphoma and high-grade glioma with dynamic susceptibility contrast-enhanced perfusion magnetic resonance imaging. Acta Radiol 2008;1–9.
69. Sugahara T, Korogi Y, Shigematsu Y, et al. Value of dynamic susceptibility contrast magnetic resonance imaging in the evaluation of intracranial tumors. Top Magn Reson Imaging 1999;10:114–24.
70. Zhu XP, Li KL, Kamaly-Asl ID, et al. Quantification of endothelial permeability, leakage space, and blood volume in brain tumors using combined T_1 and T_2* contrast-enhanced dynamic MR imaging. J Magn Reson Imaging 2000;11:575–85.
71. Maeda M, Itoh S, Kimura H, et al. Vascularity of meningiomas and neuromas: assessment with dynamic susceptibility-contrast MR imaging. AJR Am J Roentgenol 1994;163:181–6.
72. Yrjana SK, Tuominen H, Karttunen A, et al. Low-field MR imaging of meningiomas including dynamic contrast enhancement study: evaluation of surgical and histopathologic characteristics. AJNR Am J Neuroradiol 2006;27:2128–34.
73. Cha S. Update on brain tumor imaging: from anatomy to physiology. AJNR Am J Neuroradiol 2006;27:475–87.
74. Hakyemez B, Yildirim N, Erdogan C, et al. Meningiomas with conventional MRI findings resembling intraaxial tumors: can perfusion-weighted MRI be helpful in differentiation? Neuroradiology 2006;48:695–702.
75. Silva AC, Kim SG, Garwood M. Imaging blood flow in brain tumors using arterial spin labeling. Magn Reson Med 2000;44:169–73.
76. Kimura H, Takeuchi H, Koshimoto Y, et al. Perfusion imaging of meningioma by using continuous arterial spin-labeling: comparison with dynamic susceptibility-weighted contrast-enhanced MR images and histopathologic features. AJNR Am J Neuroradiol 2006;27:85–93.
77. Warmuth C, Gunther M, Zimmer C. Quantification of blood flow in brain tumors: comparison of arterial spin labeling and dynamic susceptibility-weighted contrast-enhanced MR imaging. Radiology 2003;228:523–32.
78. Yang S, Law M, Zagzag D, et al. Dynamic contrast-enhanced perfusion MR imaging measurements of endothelial permeability: differentiation between atypical and typical meningiomas. AJNR Am J Neuroradiol 2003;24:1554–9.
79. Noguchi T, Yoshiura T, Hiwatashi A, et al. Perfusion imaging of brain tumors using arterial spin-labeling: correlation with histopathologic vascular density. AJNR Am J Neuroradiol 2008;29:688–93.
80. Weber MA, Zoubaa S, Schlieter M, et al. Diagnostic performance of spectroscopic and perfusion MRI for distinction of brain tumors. Neurology 2006;66:1899–906.
81. Ludemann L, Grieger W, Wurm R, et al. Quantitative measurement of leakage volume and permeability in gliomas, meningiomas and brain metastases with dynamic contrast-enhanced MRI. Magn Reson Imaging 2005;23: 833–41.
82. Erdogan C, Hakyemez B, Yildirim N, et al. Brain abscess and cystic brain tumor: discrimination with dynamic susceptibility contrast perfusion-weighted MRI. J Comput Assist Tomogr 2005;29:663–7.
83. Holmes TM, Petrella JR, Provenzale JM Distinction between cerebral abscesses and high-grade neoplasms by dynamic susceptibility contrast perfusion MRI. AJR Am J Roentgenol 2004;183:1247–52.
84. Law M, Yang S, Babb JS, et al. Comparison of cerebral blood volume and vascular permeability from dynamic susceptibility contrast-enhanced perfusion MR imaging with glioma grade. AJNR Am J Neuroradiol 2004;25:746–55.
85. Bink A, Gaa J, Franz K, et al. Importance of diffusion-weighted imaging in the diagnosis of cystic brain tumors and intracerebral abscesses. Zentralbl Neurochir 2005;66: 119–25.
86. Mascalchi M, Filippi M, Floris R, et al. Diffusion-weighted MR of the brain: methodology and clinical application. Radiol Med (Torino) 2005;109:155–97.
87. Haris M, Gupta RK, Singh A, et al. Differentiation of infective from neoplastic brain lesions by dynamic contrast-enhanced MRI. Neuroradiology 2008;50:531–40.
88. Liebsch R, Kornhuber ME, Dietl D, et al. Blood-CSF barrier integrity in multiple sclerosis. Acta Neurol Scand 1996;94: 404–10.
89. Su JJ, Osoegawa M, Matsuoka T, et al. Upregulation of vascular growth factors in multiple sclerosis: correlation with MRI findings. J Neurol Sci 2006;243:21–30.
90. Cha S, Pierce S, Knopp EA, et al. Dynamic contrast-enhanced T_2*-weighted MR imaging of tumefactive demyelinating lesions. AJNR Am J Neuroradiol 2001;22:1109–16.
91. Whitmore RG, Krejza J, Kapoor GS, et al. Prediction of oligodendroglial tumor subtype and grade using perfusion weighted magnetic resonance imaging. J Neurosurg 2007; 107:600–9.
92. Law M, Yang S, Wang H, et al. Glioma grading: sensitivity, specificity, and predictive values of perfusion MR imaging and proton MR spectroscopic imaging compared with

conventional MR imaging. AJNR Am J Neuroradiol 2003; 24:1989–98.
93. Shin JH, Lee HK, Kwun BD, et al. Using relative cerebral blood flow and volume to evaluate the histopathologic grade of cerebral gliomas: preliminary results. AJR Am J Roentgenol 2002;179:783–9.
94. Knopp EA, Cha S, Johnson G, et al. Glial neoplasms: dynamic contrast-enhanced T_2*-weighted MR imaging. Radiology 1999;211:791–8.
95. Ludemann L, Grieger W, Wurm R, et al. Comparison of dynamic contrast-enhanced MRI with WHO tumor grading for gliomas. Eur Radiol 2001;11:1231–41.
96. Patankar TF, Haroon HA, Mills SJ, et al. Is volume transfer coefficient (K(trans)) related to histologic grade in human gliomas? AJNR Am J Neuroradiol 2005;26:2455–65.
97. Law M, Young R, Babb J, et al. Comparing perfusion metrics obtained from a single compartment versus pharmacokinetic modeling methods using dynamic susceptibility contrast-enhanced perfusion MR imaging with glioma grade. AJNR Am J Neuroradiol 2006;27:1975–82.
98. Zonari P, Baraldi P, Crisi G. Multimodal MRI in the characterization of glial neoplasms: the combined role of single-voxel MR spectroscopy, diffusion imaging and echo-planar perfusion imaging. Neuroradiology 2007;49:795–803.
99. Emblem KE, Scheie D, Due-Tonnessen P, et al. Histogram analysis of MR imaging-derived cerebral blood volume maps: combined glioma grading and identification of low-grade oligodendroglial subtypes. AJNR Am J Neuroradiol 2008;29:1664–70.
100. Young R, Babb J, Law M, et al. Comparison of region-of-interest analysis with three different histogram analysis methods in the determination of perfusion metrics in patients with brain gliomas. J Magn Reson Imaging 2007;26:1053–63.
101. Law M, Young R, Babb J, et al. Histogram analysis versus region of interest analysis of dynamic susceptibility contrast perfusion MR imaging data in the grading of cerebral gliomas. AJNR Am J Neuroradiol 2007;28:761–6.
102. Lu H, Pollack E, Young R, et al. Predicting grade of cerebral glioma using vascular-space occupancy MR imaging. AJNR Am J Neuroradiol 2008;29:373–8.
103. Cha S, Tihan T, Crawford F, et al. Differentiation of low-grade oligodendrogliomas from low-grade astrocytomas by using quantitative blood-volume measurements derived from dynamic susceptibility contrast-enhanced MR imaging. AJNR Am J Neuroradiol 2005;26:266–73.
104. Spampinato MV, Smith JK, Kwock L, et al. Cerebral blood volume measurements and proton MR spectroscopy in grading of oligodendroglial tumors. AJR Am J Roentgenol 2007;188:204–12.
105. Ellika SK, Jain R, Patel SC, et al. Role of perfusion CT in glioma grading and comparison with conventional MR imaging features. AJNR Am J Neuroradiol 2007;28:1981–7.
106. Jain R, Ellika SK, Scarpace L, et al. Quantitative estimation of permeability surface-area product in astroglial brain tumors using perfusion CT and correlation with histopathologic grade. AJNR Am J Neuroradiol 2008;29: 694–700.
107. Bulakbasi N, Kocaoglu M, Farzaliyev A, et al. Assessment of diagnostic accuracy of perfusion MR imaging in primary and metastatic solitary malignant brain tumors. AJNR Am J Neuroradiol 2005;26:2187–99.
108. Cairncross JG, Ueki K, Zlatescu MC, et al. Specific genetic predictors of chemotherapeutic response and survival in patients with anaplastic oligodendrogliomas. J Natl Cancer Inst 1998;90:1473–9.
109. Jenkinson MD, Smith TS, Joyce KA, et al. Cerebral blood volume, genotype and chemosensitivity in oligodendroglial tumours. Neuroradiology 2006;48:703–13.
110. Law M, Brodsky JE, Babb J, et al. High cerebral blood volume in human gliomas predicts deletion of chromosome 1p: Preliminary results of molecular studies in gliomas with elevated perfusion. J Magn Reson Imaging 2007;25:1113–19.
111. Grosu AL, Souvatzoglou M, Roper B, et al. Hypoxia imaging with FAZA-PET and theoretical considerations with regard to dose painting for individualization of radiotherapy in patients with head and neck cancer. Int J Radiat Oncol Biol Phys 2007;69:541–51.
112. Grosu AL, Weber WA, Astner ST, et al. 11C-methionine PET improves the target volume delineation of meningiomas treated with stereotactic fractionated radiotherapy. Int J Radiat Oncol Biol Phys 2006;66:339–44.
113. Grosu AL, Weber WA, Franz M, et al. Reirradiation of recurrent high-grade gliomas using amino acid PET (SPECT)/CT/MRI image fusion to determine gross tumor volume for stereotactic fractionated radiotherapy. Int J Radiat Oncol Biol Phys 2005;63:511–19.
114. Di Costanzo A, Scarabino T, Trojsi F, et al. Multiparametric 3T MR approach to the assessment of cerebral gliomas: tumor extent and malignancy. Neuroradiology 2006;48: 622–31.
115. Danchaivijitr N, Waldman AD, Tozer DJ, et al. Low-grade gliomas: do changes in rCBV measurements at longitudinal perfusion-weighted MR imaging predict malignant transformation? Radiology 2008;247:170–8.
116. Siegal T, Rubinstein R, Tzuk-Shina T, et al. Utility of relative cerebral blood volume mapping derived from perfusion magnetic resonance imaging in the routine follow up of brain tumors. J Neurosurg 1997;86:22–7.
117. Law M, Oh S, Babb JS, et al. Low-grade gliomas: dynamic susceptibility-weighted contrast-enhanced perfusion MR imaging—prediction of patient clinical response. Radiology 2006;238:658–67.
118. Law M, Young RJ, Babb JS, et al. Gliomas: predicting time to progression or survival with cerebral blood volume measurements at dynamic susceptibility-weighted contrast-enhanced perfusion MR imaging. Radiology 2008; 247:490–8.
119. Leimgruber A, Ostermann S, Yeon EJ, et al. Perfusion and diffusion MRI of glioblastoma progression in a four-year prospective temozolomide clinical trial. Int J Radiat Oncol Biol Phys 2006;64:869–75.
120. Li KL, Zhu XP, Checkley DR, et al. Simultaneous mapping of blood volume and endothelial permeability surface area product in gliomas using iterative analysis of first-pass dynamic contrast enhanced MRI data. Br J Radiol 2003; 76:39–50.
121. Mills SJ, Patankar TA, Haroon HA, et al. Do cerebral blood volume and contrast transfer coefficient predict prognosis in human glioma? AJNR Am J Neuroradiol 2006;27:853–8.
122. De Witte O, Oulad Ben Taib N, Branle F, et al. Contribution of PET to the management of patients with low-grade glioma. Neurochirurgie 2004;50:468–73. [In French].
123. de Wit MC, de Bruin HG, Eijkenboom W, et al. Immediate post-radiotherapy changes in malignant glioma can mimic tumor progression. Neurology 2004;63:535–7.
124. Taal W, Brandsma D, de Bruin HG, et al. Incidence of early pseudo-progression in a cohort of malignant glioma patients treated with chemoirradiation with temozolomide. Cancer 2008;113:405–10.
125. Brandes AA, Franceschi E, Tosoni A, et al. MGMT promoter methylation status can predict the incidence and outcome of pseudoprogression after concomitant radiochemotherapy in newly diagnosed glioblastoma patients. J Clin Oncol 2008;26:2192–7.
126. Chamberlain MC, Glantz MJ, Chalmers L, et al. Early necrosis following concurrent Temodar and radiotherapy in patients with glioblastoma. J Neurooncol 2007;82:81–3.

127. Schwartz RB, Carvalho PA, Alexander E, 3rd, et al. Radiation necrosis vs high-grade recurrent glioma: differentiation by using dual-isotope SPECT with 201TI and 99mTc-HMPAO. AJNR Am J Neuroradiol 1991;12: 1187–92.
128. Turner CD, Chi S, Marcus KJ, et al. Phase II study of thalidomide and radiation in children with newly diagnosed brain stem gliomas and glioblastoma multiforme. J Neurooncol 2007;82:95–101.
129. Sugahara T, Korogi Y, Tomiguchi S, et al. Posttherapeutic intraaxial brain tumor: the value of perfusion-sensitive contrast-enhanced MR imaging for differentiating tumor recurrence from nonneoplastic contrast-enhancing tissue. AJNR Am J Neuroradiol 2000;21:901–9.
130. Rock JP, Hearshen D, Scarpace L, et al. Correlations between magnetic resonance spectroscopy and image-guided histopathology, with special attention to radiation necrosis. Neurosurgery 2002;51:912–9; discussion 919–20.
131. Rock JP, Scarpace L, Hearshen D, et al. Associations among magnetic resonance spectroscopy, apparent diffusion coefficients, and image-guided histopathology with special attention to radiation necrosis. Neurosurgery 2004;54:1111–7; discussion 1117–19.
132. Chan YL, Yeung DK, Leung SF, et al. Diffusion-weighted magnetic resonance imaging in radiation-induced cerebral necrosis. Apparent diffusion coefficient in lesion components. J Comput Assist Tomogr 2003;27:674–80.
133. Hein PA, Eskey CJ, Dunn JF, et al. Diffusion-weighted imaging in the follow-up of treated high-grade gliomas: tumor recurrence versus radiation injury. AJNR Am J Neuroradiol 2004;25:201–9.
134. Zeng QS, Li CF, Liu H, et al. Distinction between recurrent glioma and radiation injury using magnetic resonance spectroscopy in combination with diffusion-weighted imaging. Int J Radiat Oncol Biol Phys 2007;68:151–8.
135. Ricci PE, Karis JP, Heiserman JE, et al. Differentiating recurrent tumor from radiation necrosis: time for re-evaluation of positron emission tomography? AJNR Am J Neuroradiol 1998;19:407–13.
136. Jain R, Scarpace L, Ellika S, et al. First-pass perfusion computed tomography: initial experience in differentiating recurrent brain tumors from radiation effects and radiation necrosis. Neurosurgery 2007;61:778–86; discussion 786–7.
137. Hu L, Baxter L, Smith K, et al. Relative Cerebral Blood Volume Values to Differentiate High-grade glioma recurrence from posttreatment radiation effect: direct correlation between image-guided tissue histopathology and localized dynamic susceptibility-weighted contrast-enhanced perfusion MR imaging measurements. AJNR Am J Neuroradiol 2009;30:552–8.
138. Cao Y, Tsien CI, Nagesh V, et al. Survival prediction in high-grade gliomas by MRI perfusion before and during early stage of RT [corrected]. Int J Radiat Oncol Biol Phys 2006;64:876–85.
139. Essig M, Waschkies M, Wenz F, et al. Assessment of brain metastases with dynamic susceptibility-weighted contrast-enhanced MR imaging: initial results. Radiology 2003; 228:193–9.
140. Lee MC, Cha S, Chang SM, et al. Dynamic susceptibility contrast perfusion imaging of radiation effects in normal-appearing brain tissue: changes in the first-pass and recirculation phases. J Magn Reson Imaging 2005;21:683–93.
141. Fuss M, Wenz F, Scholdei R, et al. Radiation-induced regional cerebral blood volume (rCBV) changes in normal brain and low-grade astrocytomas: quantification and time and dose-dependent occurrence. Int J Radiat Oncol Biol Phys 2000;48:53–8.
142. Price SJ, Jena R, Green HA, et al. Early radiotherapy dose response and lack of hypersensitivity effect in normal brain tissue: a sequential dynamic susceptibility imaging study of cerebral perfusion. Clin Oncol (R Coll Radiol) 2007;19:577–87.
143. Cao Y, Tsien CI, Shen Z, et al. Use of magnetic resonance imaging to assess blood-brain/blood-glioma barrier opening during conformal radiotherapy. J Clin Oncol 2005;23: 4127–36.
144. Behrens PF, Ostertag CB, Warnke PC. Regional cerebral blood flow in peritumoral brain edema during dexamethasone treatment: a xenon-enhanced computed tomographic study. Neurosurgery 1998;43:235–40; discussion 240–1.
145. Bastin ME, Carpenter TK, Armitage PA, et al. Effects of dexamethasone on cerebral perfusion and water diffusion in patients with high-grade glioma. AJNR Am J Neuroradiol 2006;27:402–8.
146. Jager HR, Waldman AD, Benton C, et al. Differential chemosensitivity of tumor components in a malignant oligodendroglioma: assessment with diffusion-weighted, perfusion-weighted, and serial volumetric MR imaging. AJNR Am J Neuroradiol 2005;26:274–8.
147. Folkman J. Tumor angiogenesis: therapeutic implications. N Engl J Med 1971;285:1182–6.
148. Folkman J. Angiogenesis: an organizing principle for drug discovery? Nat Rev Drug Discov 2007;6:273–86.
149. Carmeliet P, Jain RK. Angiogenesis in cancer and other diseases. Nature 2000;407:249–57.
150. O'Connor JP, Jackson A, Parker GJ, et al. DCE-MRI biomarkers in the clinical evaluation of antiangiogenic and vascular disrupting agents. Br J Cancer 2007;96: 189–95.
151. Vredenburgh JJ, Desjardins A, Herndon JE, 2nd, et al. Phase II trial of bevacizumab and irinotecan in recurrent malignant glioma. Clin Cancer Res 2007;13:1253–9.
152. Sathornsumetee S, Cao Y, Marcello JE, et al. Tumor angiogenic and hypoxic profiles predict radiographic response and survival in malignant astrocytoma patients treated with bevacizumab and irinotecan. J Clin Oncol 2008;26:271–8.
153. Gossmann A, Helbich TH, Kuriyama N, et al. Dynamic contrast-enhanced magnetic resonance imaging as a surrogate marker of tumor response to anti-angiogenic therapy in a xenograft model of glioblastoma multiforme. J Magn Reson Imaging 2002;15:233–40.
154. Cha S, Knopp EA, Johnson G, et al. Dynamic contrast-enhanced T_2-weighted MR imaging of recurrent malignant gliomas treated with thalidomide and carboplatin. AJNR Am J Neuroradiol 2000;21:881–90.
155. Akella NS, Twieg DB, Mikkelsen T, et al. Assessment of brain tumor angiogenesis inhibitors using perfusion magnetic resonance imaging: quality and analysis results of a phase I trial. J Magn Reson Imaging 2004;20:913–22.
156. Nabors LB, Mikkelsen T, Rosenfeld SS, et al. Phase I and correlative biology study of cilengitide in patients with recurrent malignant glioma. J Clin Oncol 2007;25:1651–7.
157. Batchelor TT, Sorensen AG, di Tomaso E, et al. AZD2171, a pan-VEGF receptor tyrosine kinase inhibitor, normalizes tumor vasculature and alleviates edema in glioblastoma patients. Cancer Cell 2007;11:83–95.
158. Schnell O, Krebs B, Carlsen J, Miederer L, Goetz C, Goldbrunner RH, et al. Imaging of integrin alpha(v)beta(3) expression in patients with malignant glioma by [18F] Galacto-RGD positron emission tomography. Neuro Oncol 2009;11:861–70.
159. Jain RK, di Tomaso E, Duda DG, Loeffler JS, Sorensen AG, Batchelor TT. Angiogenesis in brain tumours. Nat Rev Neurosci 2007;8:610–22.
160. O'Connor JP, Naish JH, Parker GJ, Waterton JC, Watson Y, Jayson GC, et al. Preliminary study of oxygen-enhanced longitudinal relaxation in MRI: a potential novel biomarker of oxygenation changes in solid tumors. Int J Radiat Oncol Biol Phys 2009;75:1209–15.